

We are IntechOpen, the world's leading publisher of Open Access books Built by scientists, for scientists

6,300

Open access books available

171,000

International authors and editors

190M

Downloads

Our authors are among the

154

Countries delivered to

TOP 1%

most cited scientists

12.2%

Contributors from top 500 universities



WEB OF SCIENCE™

Selection of our books indexed in the Book Citation Index
in Web of Science™ Core Collection (BKCI)

Interested in publishing with us?
Contact book.department@intechopen.com

Numbers displayed above are based on latest data collected.
For more information visit www.intechopen.com



Research of M-PAM and Duobinary Modulation Formats for Use in High-Speed WDM-PON Systems

Toms Salgals, Inna Kurbatska, Sandis Spolitis, Vjaceslavs Bobrovs and Girts Ivanovs

Abstract

The exponential growth of Internet data traffic and progress of Information and Communication Technology (ICT) sector pushes hard the telecommunication infrastructure for upgrading the transmission data rate. Wavelength division multiplexed passive optical networks (WDM-PONs) can be the next generation solution for nowadays problems which are related to transmission capacity. Next-generation WDM-PON systems based on mixed wavelength transmitters are expected to become more cost-efficient at high per user data rates, e.g., over 10 Gbit/s per channel. Important advantage of this technology is to set various channel spacing and use different modulation formats to increase spectral efficiency in the same time and provide different transmission speeds for end user, based on pay-as-you-grow approach. Therefore, several modulation formats like non-return to zero (NRZ) also called 2-level pulse-amplitude modulation (PAM-2), four level PAM or PAM-4 and Duobinary (DB) are investigated to understand their limitations, advantages and disadvantages to be further used in next generation PON systems to increase its capacity and spectral efficiency.

Keywords: wavelength division multiplexed passive optical network (WDM-PON), non-return to zero (NRZ), four level pulse-amplitude modulation (PAM-4), duobinary (DB), capacity, spectral efficiency

1. Introduction

The exponential growth of Internet data traffic and progress of Information and Communication Technology (ICT) sector pushes hard the telecommunication infrastructure for upgrading the transmission data rate [1]. Power and cost-efficient fiber optical access networks, like passive optical network (PON) and short-range fiber optical links are one of the key technologies enabling bandwidth hungry services like video on demand (VoD), high definition TV, and cloud computing supported by large scale high-performance computers and data centers. Such optical links typically use direct detection and on-off keying modulation (OOK) with NRZ line code. Today's challenge for optical access networks and data centers is to increase the serial line rate of a NRZ link meeting the requirements to the physical bandwidth of the photonic and electronic components like optical signal modulators and photodiodes [2].

Solution for telecommunication infrastructure upgrade and alternative solution for increase of the serial line rate of the NRZ link is to use multi-level signaling formats such as pulse-amplitude modulation (PAM), abbreviated as PAM-M or M-PAM, where multiple digital bits per symbol are encoded into M different signal amplitude levels. The four-level PAM modulation format is receiving significant attention because of its relative ease of implementation in comparison to higher-order modulation formats like quadrature phase-shift keying (QPSK), and m-ary quadrature amplitude modulation (m-QAM). It is clear that M-PAM offers a good trade-off between performance and complexity. Usage of PAM-4 format is effective way to double the data rate of NRZ link. Previously PAM-4 modulation formats have been investigated for application with traditional electrical networks [3, 4], but now researchers are focused on investigation of PAM-4 and M-PAM modulation formats for utilization in optical access networks as well as data center interconnections [5]. Also, there are very limited number of studies which are focused on spectrum slicing and stitching back method, which deals with bandwidth bottleneck problem by slicing the broadband signal in lower-bandwidth signal slices. This spectrum slicing and stitching back method or technique allows transmission of wide bandwidth signals from the service provider to the end user over an optical distribution network via low bandwidth equipment [6, 7]. It is ideally suited for cost sensitive fiber optical access networks where variable bandwidth and scalability as well as flexibility are important. It must be noted that this method is investigated for intensity modulated direct detection NRZ-OOK and duobinary systems, but there are no investigations on its usage together with M-PAM systems [8, 9]. It must be noted that multi-level signaling also changes some rules, which were used in NRZ coded transmission systems. For M-PAM systems it is important to implement more complex and precise level threshold detection for signal inputs, also signal-to-noise (SNR) requirements are higher than in case of NRZ. Eye time skew, amplitude compression in lower eye diagram eyes, intersymbol interference for M-PAM systems also is an issue which must be investigated. So, we can say that PAM-4 links are new science—still learning what impairments create errors in receivers [10, 11]. Significant efforts have been put on investigation of PAM-4 format in fiber optical transmission networks, however there are following aspects, which have not been studied or have been studied insufficiently. High-level PAM modulation techniques, like PAM-4, can dramatically improve the spectral efficiency and available bitrate by using the bandwidth of already existing optical, electro-optical or electrical devices. Minimal available channel spacing (which has direct impact on the utilization of resources like optical spectrum), maximal available number of channels, by wavelength division multiplexing (WDM) technique, maximal transmission distance (network reach) in dispersion compensated and non-compensated M-PAM modulated WDM-PON optical access systems.

Another way to improve capacity of limited bandwidth is by using duobinary modulation format. Transmission capacity will be increased in comparison with NRZ, utilization of DB will increase the transmission capacity by improving the bandwidth efficiency and reducing channel spacing with this modulation format [12]. Duobinary modulation format is type of proficient pseudo-multilevel modulation format, and therefore is the area of interest due to its increased spectral efficiency. It has been already used to increase the channel capacity by improving the bandwidth utilization in commercial links. The most important feature of duobinary modulation format is its usage for longer transmission distances where it has high tolerance to the influence of chromatic dispersion (CD) [13].

At first, in the paper we investigate the performance and minimal channel interval of 10 Gbit/s per channel NRZ-OOK (which is basically PAM-2) modulated transmission system, then we investigate PAM-4 and raise the transmission speed up to 20 Gbit/s per wavelength and in the end compare it to NRZ and duobinary modulation formats.

2. Evaluation of various channel spacings for increasing spectral efficiency of WDM-PON transmission system

At the moment passive optical networks have been standardized to next-generation NG-PON2 accordingly to ITU-T G.989.2 recommendation standards and are widely investigated. Operators are widely deploying time-division multiplexing (TDM) based passive optical networks in urban areas with bitrates up to 10 Gbit/s, but WDM-PON's still are in stage of research [14, 15].

The ITU-T G.694.1 recommendation provides a frequency grid for (WDM) transmission systems and specifies inter-channel intervals. The same frequency grid or channel spacing is used for spectral effectiveness improvement of PON system in our research. Anchored to 193.1 THz (central channel frequency), it supports a variety of inter-mediate channel spacings ranging from narrowed 12.5 GHz to 100 GHz and wider. Depending on the selected step of the inter-channel interval are defined the following abbreviations and acronyms:

- WDM—wavelength division multiplexing.
- CWDM—coarse wavelength division multiplexing.
- DWDM—dense wavelength division multiplexing.

There are two types of inter-channel interval definitions in (WDM) systems:

- Fixed inter-channel interval (fixed grid).
- Flexible inter-channel interval (flexible grid).

According to ITU-T G.694.1 rec. the minimum step of a fixed channel interval is 12.5 GHz (please see **Table 1**). The flexible channel step is half of the 12.5 GHz, that can be used for the inter-channel interval like 6.25 GHz. Reducing the inter-channel interval leads to increase of crosstalk and non-linear effects (NOE) of transmitted optical signal [16–18].

For research of spectral efficiency increasing, the experimental 2-channel NRZ-OOK modulated 10 Gbit/s bit rate per channel transmission system model was created for Next-generation WDM-PON systems based on tunable wavelength transmitters, please see in **Figure 1**. First step of the research is based on various channel spacing impact on the end user transmitted signal with following fixed 10 Gbit/s transmission speed per channel.

As one can see in **Figure 1**. transmitter (Tx) part of our investigated transmission system model consists of two continuous wave (CW) laser sources—Agilent 81949A, with fixed central frequency 193.1 THz or 1552.524 nm in wavelength, and COBRITE DX-1 laser with tunable central frequency, which can be set the necessary channel spacing. Agilent 81949A continuous wave laser source was connected

Nominal central frequencies (THz) for spacing				Nominal central wavelengths (λ , nm)
12.5 GHz	25 GHz	50 GHz	100 GHz	
193.9375	-	-	-	1530.0413
195.9250	195.925	-	-	1530.1389
195.9125	-	-	-	1530.2365
195.9000	195.900	195.90	195.9	1530.3341

Table 1.
 Nominal central frequencies grid of the DWDM grid [17].

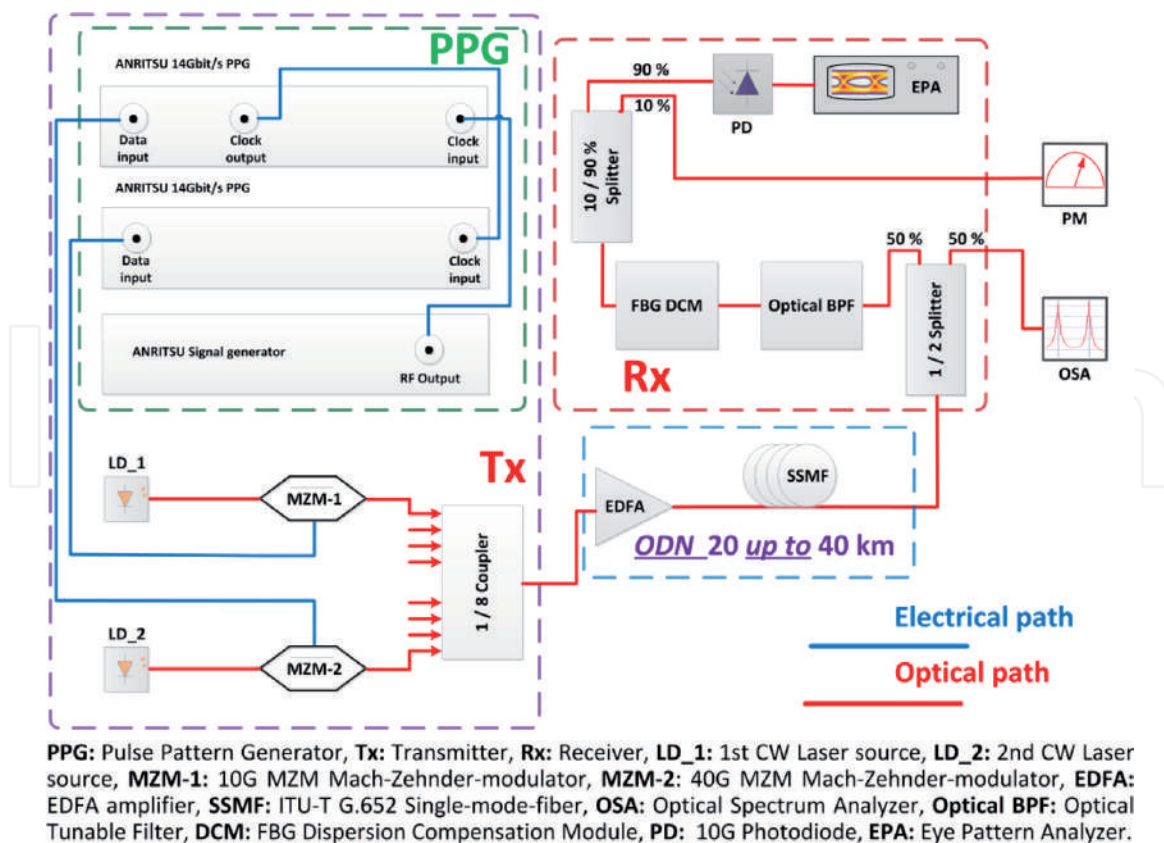


Figure 1.

2-Channel NRZ-OOK modulated optical transmission system with 10 Gbit/s transmission speed per channel and flexible channel spacing.

to the 40G intensity Mach-Zehnder (MZM) modulator, COBRITE DX-1 laser light source was connected to the second MZM intensity modulator. Both laser sources were used with minimal output power +9 dBm for Agilent 81949A and +6 dBm for COBRITE DX-1. To provide the same level of optical power for both optical channels, after the PHOTLINE 40G MZM, an optical attenuator of 3.05 dB insertion loss was additionally attached to the modulator's optical output. Pulse Pattern Generator (PPG) with Pseudo random bit sequence (PRBS9) was used for generation of NRZ coded electrical signals. The external 10 GHz clock signal generator was used in this experiment for as a clock signal source for PPGs. Two electrical PPG non-inverted RF data signal outputs were connected to each of MZMs electrical signal inputs. The data rate for each of the PPGs was 10 Gbit/s throughout the experiment.

ITU-T G.652 standard single mode fiber (SSMF) with dispersion coefficient of 16 ps/(nm × km), and 0.2 dB/km attenuation coefficient was used in optical distribution network. Depending of SSMF fiber span length (20 or 40 km), an Erbium doped fiber amplifier (EDFA) with additional gain was used to provide sufficient optical power level before the PIN photoreceiver.

At the receiver part (Rx), the incoming optical signal was divided by 50% power splitter with 3.5 dB insertion loss. One output of optical power splitter was connected to the optical spectrum analyzer (OSA). Second output of power splitter was connected to the optical band pass filter (BPF) OTF-350 with a tuned 35 GHz 3-dB bandwidth. After BPF filter, fiber Bragg grating dispersion compensation module (FBG DCM), with 3 dB insertion loss was connected for post-compensation purposes of chromatic dispersion (CD). To avoid the maximum optical input optical power level rating of +3 dBm before the 10G PIN photoreceiver (PD) a monitoring power splitter with a power ratio of 10–90% and power meter was used. First channel was filtered out by using optical BPF. As one can see in **Figure 2(a)**, optical spectrum with central channel frequency 1552.560 nm (193.096 THz in frequency)

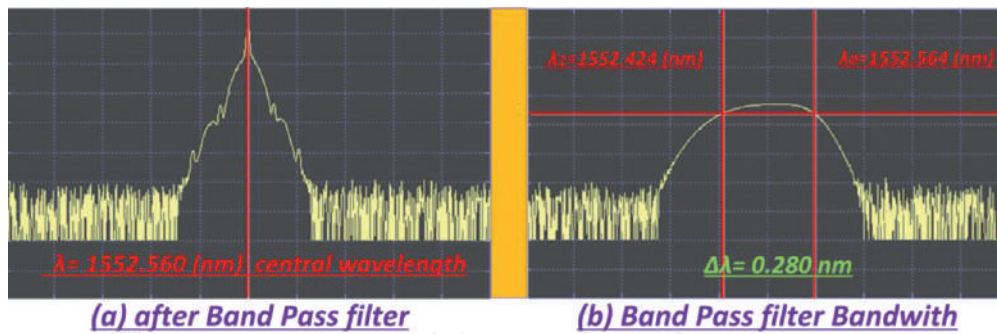


Figure 2. Central channel spectrum of 2-channel NRZ-OOK modulated optical transmission system with 10 Gbit/s per channel: (a) after BPF and (b) measured amplified frequency response of BPF.

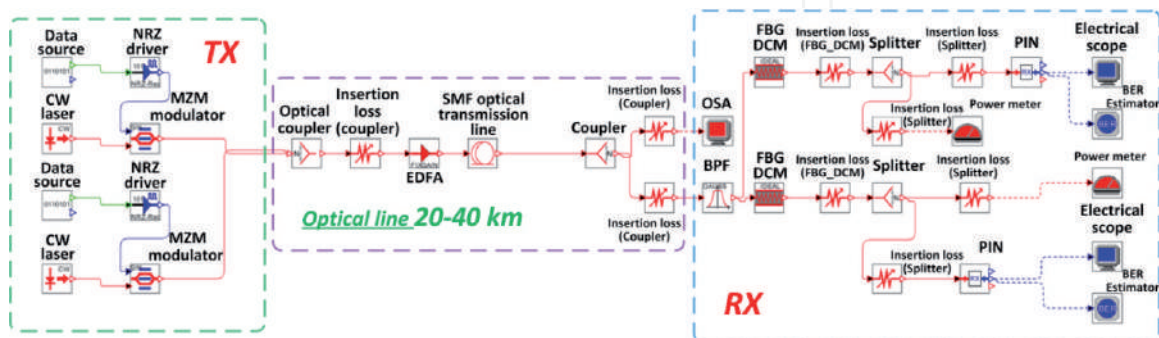


Figure 3. Simulation scheme of 2-channel NRZ modulated optical transmission system with 10 Gbit/s transmission speed per channel with flexible channel interval.

is slightly shifted relative to ITU-T G.694.1 rec. Grid central frequency of 193.1 THz. By obtained results from the optical spectrum analyzer (OSA), the BPF pass band is $\Delta\lambda = 0.280$ nm equal to 35 GHz, where $\lambda_0 = 1552.564$ nm and $\lambda_1 = 1552.424$ nm.

An eye analyzer was used for measurements of received electrical signal quality. The eyes of received signals for both channels were open, therefore leading to error free transmission. As the eye pattern analyzer for quality measurement use special masks to determine if the signal is above or below necessary quality. We continued our research in OptSim simulation environment by creating relevant simulation model and using the previously obtained experimental data.

For more precise expected Bit-error-rate (BER) values of received signal the simulation model was created in OptSim simulation software environment. The model used BER estimator based on statistical signal analysis. As one can see in **Figure 3**, simulation scheme implemented in OptSim simulation software for BER measurements has the same setup as experimental system. In the OptSim simulation environment, it is necessary to perform the assembly of used electrical-optical components in order to repeat the 2-channel NRZ-OOK modulated 10 Gbit/s per channel transmission system to research impact of various channel spacings.

According to ITU-T G.694.1 rec., see **Table 2**, during the experiment, the inter-channel interval for transmission system was changed from 100 GHz to 25 GHz. We started the experiment at a 20 km long fiber ODN distance with 100 GHz channel spacing. Firstly, the measurements was carried out without the chromatic dispersion (CD) post-compensation, at 20 km fiber link. For transmission over 20 km fiber span we observed negligible chromatic dispersion impact on 10 Gbit/s signal, received signal is mainly insignificant impact of dispersion [19].

The 12.5 GHz channel spacing interval was not obtained in this step of research. The reason for that was too wide filter pass-band, as a result photoreceiver captured

Frequency interval (THz)	100 GHz		50 GHz		25 GHz	
	Freq., (THz)	(λ , nm)	Freq., (THz)	(λ , nm)	Freq., (THz)	(λ , nm)
1st CH	193.1	1552.524	193.1	1552.524	193.1	1552.524
2nd CH	193.0	1553.328	193.05	1552.926	193.075	1552.725

Table 2.
Experimentally used channel interval according to ITU-T G.694.1 rec.

1st-CH, (THz)	2nd-CH, (THz)	2nd-CH, (nm)	Delta, (THz)	CH-interval, (GHz)
193.1	193.08125	1552.675	0.01875	18.750
193.1	193.07813	1552.700	0.02187	21.875
193.1	193.07500	1552.725	0.02500	25.000
193.1	193.07188	1552.751	0.02187	28.125
193.1	193.06875	1552.776	0.03125	31.250
193.1	193.06563	1552.801	0.02187	34.375
193.1	193.06250	1552.826	0.03750	37.500
193.1	193.05625	1552.876	0.04375	43.750
193.1	193.05000	1552.926	0.05000	50.000
193.1	193.00000	1553.329	0.10000	100.000

Table 3.
Channel spacing dependence on the channel interval.

both channels simultaneously. They did not appear on the Eye Analyzer because it was not possible to synchronize between the transmitter and receiver. After obtaining the results at fixed inter-channel intervals from 100 to 25 GHz, the smallest inter-channel interval at which transmission is possible was found. The step used to search for the inter-channel interval is 6.25 GHz and half of the found step $6.25/2 = 3.125$ GHz. Result of channel spacing impact was obtained from channel with fixed central frequency of 193.1 THz = 1552.524 wavelength corresponding to the laser source used by Agilent 81949A. Our transmission system has only two channels, it is not possible to choose a central channel, both channels have mainly the same effect of crosstalk. The channel interval was changed by changing the central wavelength of the second CW laser source with 6.25 and 3.125 GHz step. Instead of experiment for 2-channel NRZ-OOK modulated optical transmission system with 10 Gbit/s transmission speed per channel previously calculated flexible channel interval was used in our research, please see **Table 3**.

Fiber optical transmission system made by the optical components affected by various factors caused by higher attenuation mentioned in specification insertion loss. To create same simulation model in OptSim simulation software environment, it was necessary to adapt model optical elements of the actual loss. In **Figure 4**, we can see BER estimated from the data obtained in OptSim simulation according to different channel intervals.

The BER threshold of 10^{-9} for our investigated transmission system was used to evaluate maximal crosstalk impact between the channels. According to the

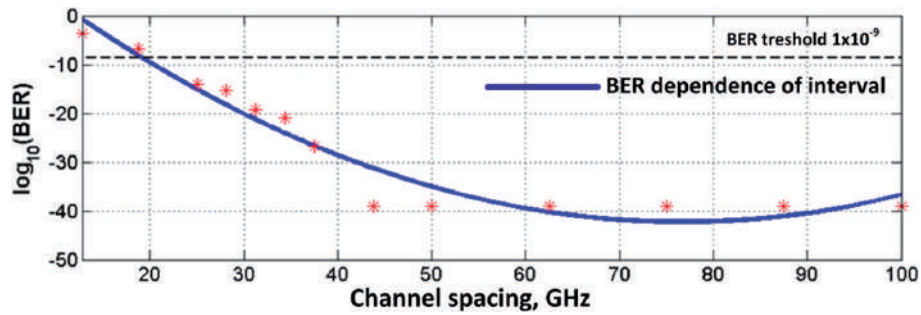


Figure 4. BER dependence on the channel interval for a 20 km long 2-channel NRZ-OOK modulated optical transmission system with 10 Gbit/s transmission speed per channel.

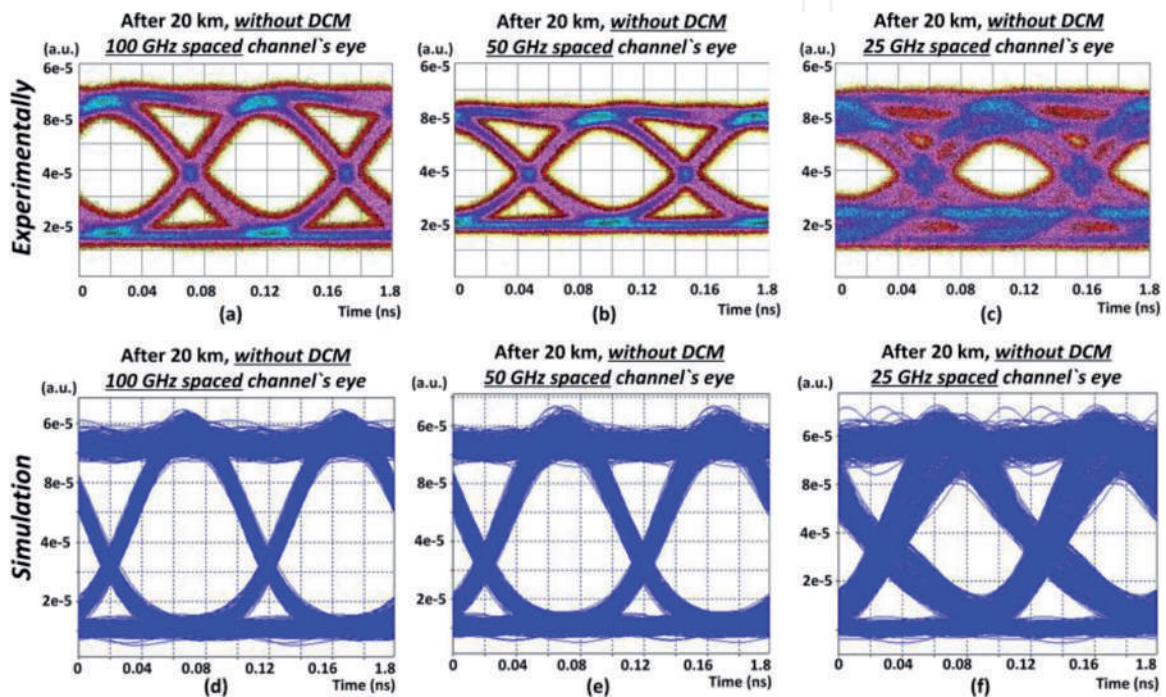


Figure 5. Comparison of experimental and simulation results: eye diagrams of 20 km 2-channel NRZ-OOK modulated optical transmission system with 10 Gbit/s transmission speed per channel without CD post-compensation: (a) 100 GHz channel spacing, (b) 50 GHz channel spacing, (c) 25 GHz channel spacing, (d) 100 GHz channel spacing in the environment of OptSim, (e) 50 GHz channel spacing in the environment of OptSim, and (f) 25 GHz channel spacing in the environment of OptSim.

obtained results channel interval effect up to 30 GHz can be evaluated, higher than used value of BPF filter. Deterioration of the BER used for channel interval less than 30 GHz in our research, can be explained by adjacent channel overlapping. At 20 km long SSMF fiber optical link minimal channel spacing was achieved ensuring $BER < 10^{-3}$ threshold at 25 GHz. In **Figure 5**, we can see experimental and theoretical (simulation data) eye diagrams of received signal for second channel with 100, 50 and 25 GHz channel spacing crosstalk impact, please see **Figure 5**.

In second part of our research the length of ODN was increased from 20 to 40 km, by adding 20 km SSMF fiber span. The effect of chromatic dispersion was observed in upgraded transmission system. Fiber Bragg grating dispersion compensation module (FBG DCM) with -640 ps/nm was used for dispersion compensation. The BER value exceeded our defined BER threshold of 1×10^{-9} at 31.25 GHz channel spacing according to the obtained results of OptSim simulation software. By performing experiment, the 31.25 GHz inter-channel spacing was the last interval at which mask testing with eye diagram analyzer for received eye diagrams was

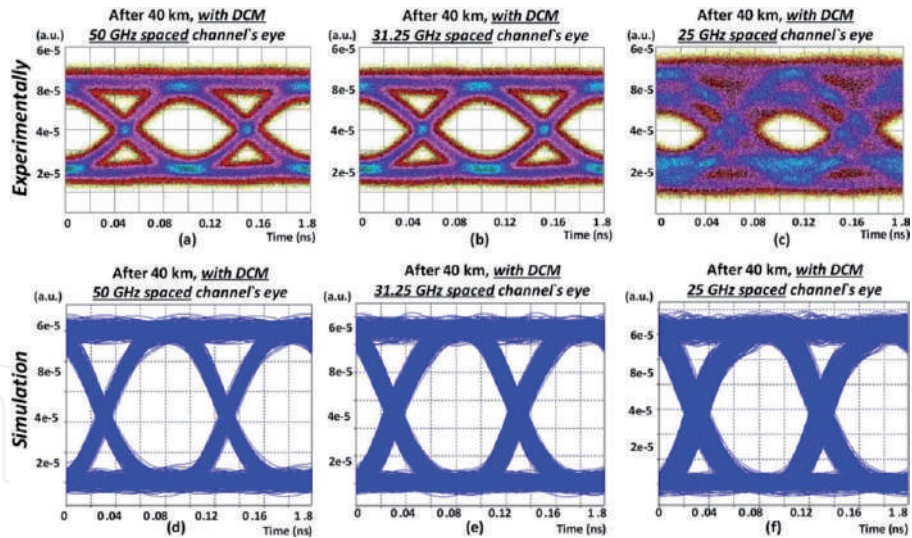


Figure 6. Comparison of experimental and simulation results: eye diagrams of 40 km 2-channel NRZ modulated optical transmission system with 10 Gbit/s transmission speed per channel with CD post-compensation: (a) 50 GHz channel spacing, (b) 31.25 GHz channel spacing, (c) 25 GHz channel spacing, (d) 50 GHz channel spacing in the environment of OptSim, (e) 31.25 GHz channel spacing in the environment of OptSim, and (f) 25 GHz channel spacing in the environment of OptSim.

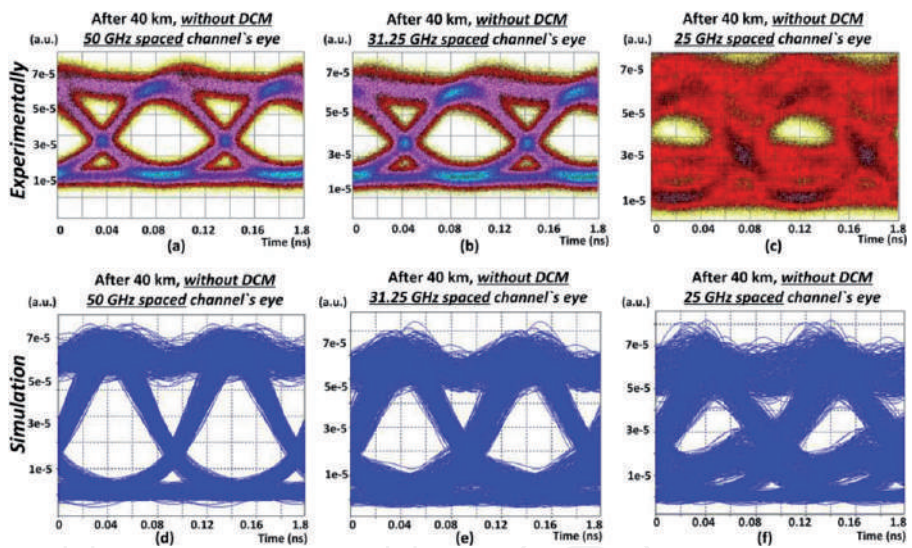


Figure 7. Comparison of experimental and simulation results: eye diagrams of 40 km 2-channel NRZ modulated optical transmission system with 10 Gbit/s transmission speed per channel without CD post-compensation: (a) 50 GHz channel spacing, (b) 31.25 GHz channel spacing, (c) 25 GHz channel spacing, (d) 50 GHz channel spacing in the environment of OptSim, (e) 31.25 GHz channel spacing in the environment of OptSim, and (f) 25 GHz channel spacing in the environment of OptSim.

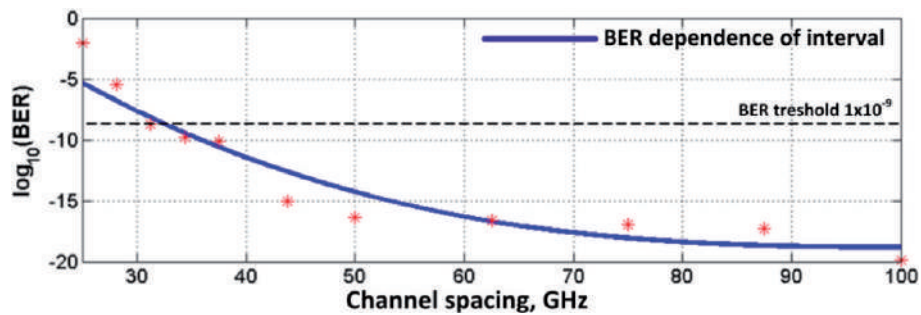


Figure 8. BER dependence on channel interval for a 40 km 2-channel NRZ-OOK modulated optical transmission system with 10 Gbit/s transmission speed per channel.

possible [20]. By obtained experimental and simulation results it can be concluded that the model of optical transmission created in the simulation environment corresponds to the experimental fiber optic transmission system. Channel overlaps at 40 km long fiber section, with use of dispersion compensation, see **Figure 6** and without dispersion compensation see **Figure 7**. Results, with BER below our inter-channel interval, please see **Figure 8**.

Our defined BER threshold of 1×10^{-9} was exceeded at the 31.25 GHz channel interval where the BER of received signal was 7.4×10^{-11} .

3. Evaluation of PAM-4 modulation format use in WDM-PON systems

In our research we investigated the 4-channel 10 Gbaud/s (20 Gbit/s) per channel PAM-4 modulated WDM-PON access system with minimal allowable channel spacing, which has a direct impact on the utilization of resources like optical spectrum. The research was made with and without fiber chromatic dispersion (CD) fiber Bragg grating compensation module (FBG DCM). We evaluate system performance and found the maximal transmission distance for multichannel PAM-4 modulated WDM-PON transmission system operating at 20 Gbit/s per channel. In OptSim simulation software we created transmission system model to evaluate the performance of 4-channel PAM-4 modulated WDM-PON transmission system operating at 10 Gbaud/s or 20 Gbit/s per channel under the condition with BER threshold of 10^{-3} , by use of Reed Solomon (RS 255,223) forward error correction (FEC) code for 10 Gbit/s PONs [21, 22]. The theoretical FEC relationship restores 1.1×10^{-3} pre-FEC BER to a 10^{-12} post-FEC in the PON standards. As it is shown in **Figure 9**, the PAM-4 modulated WDM-PON simulation scheme was created in OptSim simulation software environment. Here the Matlab software was used for BER estimation of received PAM-4 signals. WDM-PON simulation model consists of 4 channels, with central frequency 193.1 THz for second channel and chosen 50 or 100 GHz, according to the previously mentioned ITU G.694.1 rec. According to our previously channel interval research of flexible channel spacing like 37.5 and 25 GHz also was realized. However, the quality of received signal was low, with crosstalk impact and error-free transmission was not possible, performance was above our defined BER threshold 1×10^{-3} .

We evaluated the performance of WDM-PON architecture in terms of maximal transmission reach. Optical line terminal (OLT) is located in central office (CO) and consists of four transmitters (OLT_Tx). Each OLT_Tx transmitter consists of two pseudo-random bit sequence (PRBS) generators and NRZ drivers, as a result two

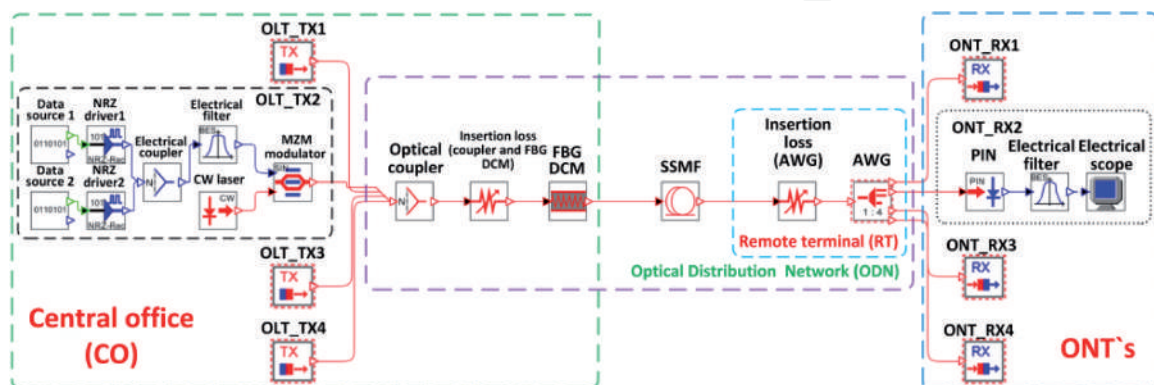


Figure 9. Simulation scheme of 4-channel PAM-4 modulated WDM-PON transmission system operating at 10 Gbaud/s per wavelength.

electrical signals are generated where one of them has twice larger amplitude than other for each particular electrical signal. An electrical coupler is used to couple both electrical signals in such a way generating electrical PAM-4 signal. Afterwards, additional electrical filters were used for ensuring of optimal system performance. Generated PAM-4 signal was send to external MZM with 3 dB insertion loss and 20 dB extinction ratio. Continuous wavelength (CW) laser with linewidth of 50 MHz and output power of +3 dBm is used as the light source [23].

Optical signals from four transmitters are coupled together by using optical coupler with 1 dB insertion loss. Chromatic dispersion pre-compensation by FBG DCM, with additional 3 dB insertion loss is realized for all channels before launching optical signal in ITU-T G.652 single mode fiber (SMF), used for transmission in optical distribution network (ODN). After transmission in ODN, all channels are separated by arrayed waveguide grating (AWG) demultiplexer which insertion loss is 3.5 dB. Here we applied various channel spacings—50 or 100 GHz (3-dB bandwidth is 20 GHz) for research of the crosstalk impact. Each receiver of optical network terminal (ONT) consists of PIN photoreceiver (sensitivity is -19 dBm for BER of 10^{-12}). An optimal electrical Bessel low-pass filter (LPF) with bandwidth (3-dB bandwidth is 7.5 GHz), was adopted for more successful system performance. An electrical scope was used for evaluation of received signal bit patterns quality, accordingly, eye diagrams.

As it is shown in **Figure 10(a)** in B2B configuration for first investigated 100 GHz channel spacing, the signal quality is good, eye is open and error-free transmission can be provided. After 59 km transmission which was the maximum transmission distance without use of FBG DCM, the BER of received signal was 7.5×10^{-4} , please see **Figure 10(b)**. Dispersion compensation FBG DCM module was implemented to evaluate transmission distance in terms of maximal reach. As it is shown in **Figure 10(c)** by using this technique of FBG DCM, the maximum achievable transmission distance 74 km was reached, where BER of received signal was 9×10^{-4} . Extra 15 km or 25.4% of link length was gained.

Therefore, basis on our research data we can conclude that narrower channel spacing for 4-channel PAM-4 10 Gbaud/s WDM-PON system is 50 GHz. As it is shown in **Figure 11(a)** in B2B configuration for second investigated 50 GHz channel spacing, the signal quality is good, eye is open and error-free transmission can be provided. After 58 km transmission, which was the maximum transmission distance without use of FBG DCM, the BER of received signal was 8×10^{-4} , shown in **Figure 11(b)**. In our research we show the eye diagrams of received signal for the second channel, the drop in BER performance can be explained by the impact of crosstalk between channels. Dispersion compensation FBG DCM module was

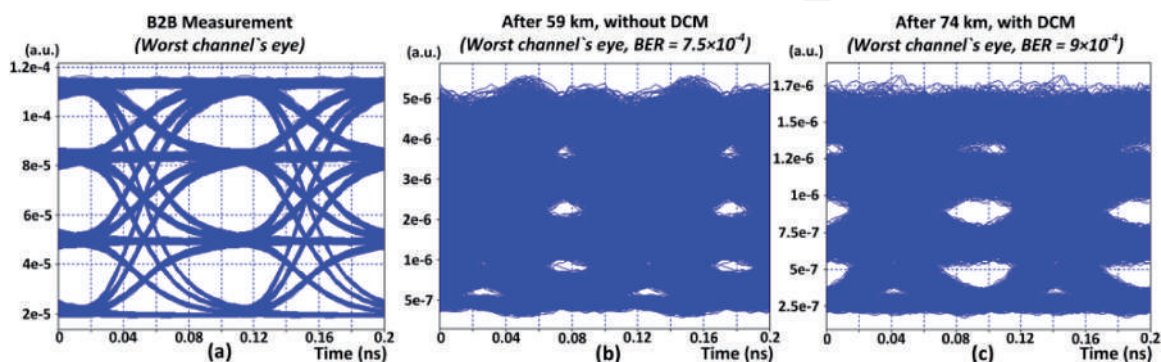


Figure 10.

Eye diagrams of received signal (a) after B2B transmission, (b) after 59 km transmission without use of CD pre-compensation, (c) after 74 km transmission with use of CD pre-compensation for 4-channel 20 Gbit/s per channel PAM-4 100 GHz spaced WDM-PON transmission system.

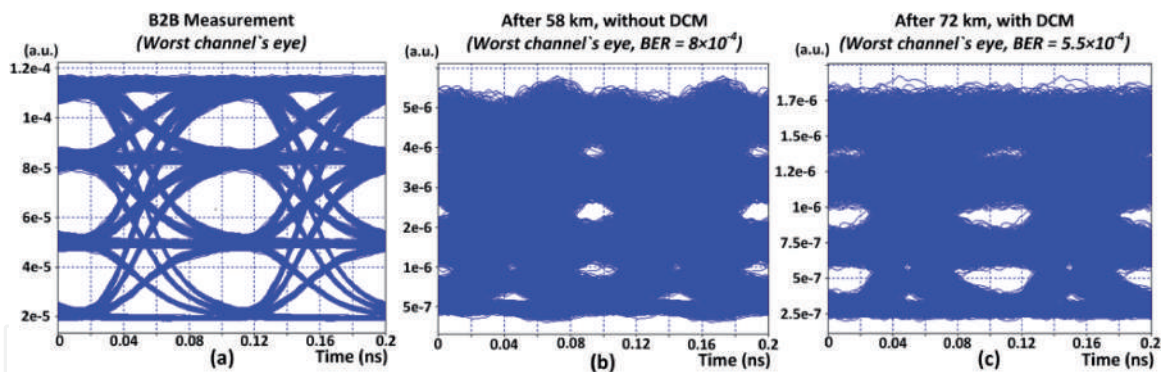


Figure 11. Eye diagrams of received signal (a) after B2B transmission, (b) after 58 km transmission without use of CD pre-compensation (c) after 72 km transmission with use of CD pre-compensation for 4-channel 20 Gbit/s per channel PAM-4 50 GHz spaced WDM-PON transmission system.

implemented to evaluate transmission distance in terms of maximal reach. As it is shown in **Figure 11(c)**, by using this technique of FBG DCM, the maximum achievable transmission distance was 72 km, with BER of received signal 5.5×10^{-4} . Extra 14 km or 24% of link length was gained.

It was shown, that maximal transmission distance with BER below FEC limit of 10^{-3} for 100 GHz spaced 4-channel PAM-4 WDM-PON system can be increased by 15 km or 25.4% by use of implemented FBG DCM. In case of 50 GHz channel spacing, maximum transmission system reach can be increased by 14 km or 24% by use of FBG DCM.

4. Evaluation of PAM-4, NRZ and duobinary modulation formats performance in WDM-PON system architecture

In case of research we improve our previously made 4-channel PAM-4 WDM-PON system simulation model capacity by increasing number of multilevel channels and implement the use of different modulation formats in terms of system performance by maximal achievable reach. Several modulation formats have been proposed in the past and have become standards. In this research are investigated several modulation formats for use in WDM-PON architecture-based system, like NRZ, PAM-4 and duobinary (DB). Alternative solution instead widely used direct detection on-off keying modulation format NRZ-OOK with physical bandwidth limitations is to use more spectrally efficient multi-level formats such as PAM-4 [24, 25]. Another way to improve the bandwidth efficiency and reduce channel spacing is by using duobinary modulation format [12]. The most important feature of this multi-level modulation format duobinary is a viability of usage for longer transmission distances without regeneration with high tolerance to chromatic dispersion CD influence. As we know duobinary is used to increase the channel capacity by improving the bandwidth utilization [13].

The goal of our created 8-channel 20 Gbit/s per channel WDM-PON simulation model evaluate maximum transmission reach using different modulation formats, discussed previously in this paper like NRZ, PAM-4 and perspective duobinary modulation format. As it is shown in **Figure 12** the 8-channel WDM-PON simulation scheme with different optical transmitters (Tx) located in CO Optical Line Terminal (OLT_Tx) part for each modulation format realization are shown. According to ITU-T G.694.1 rec. Frequency with grid central frequency of 193.1 THz and channel spacing of 50 and 100 GHz are chosen for research of crosstalk impact on modulation formats under research [26].

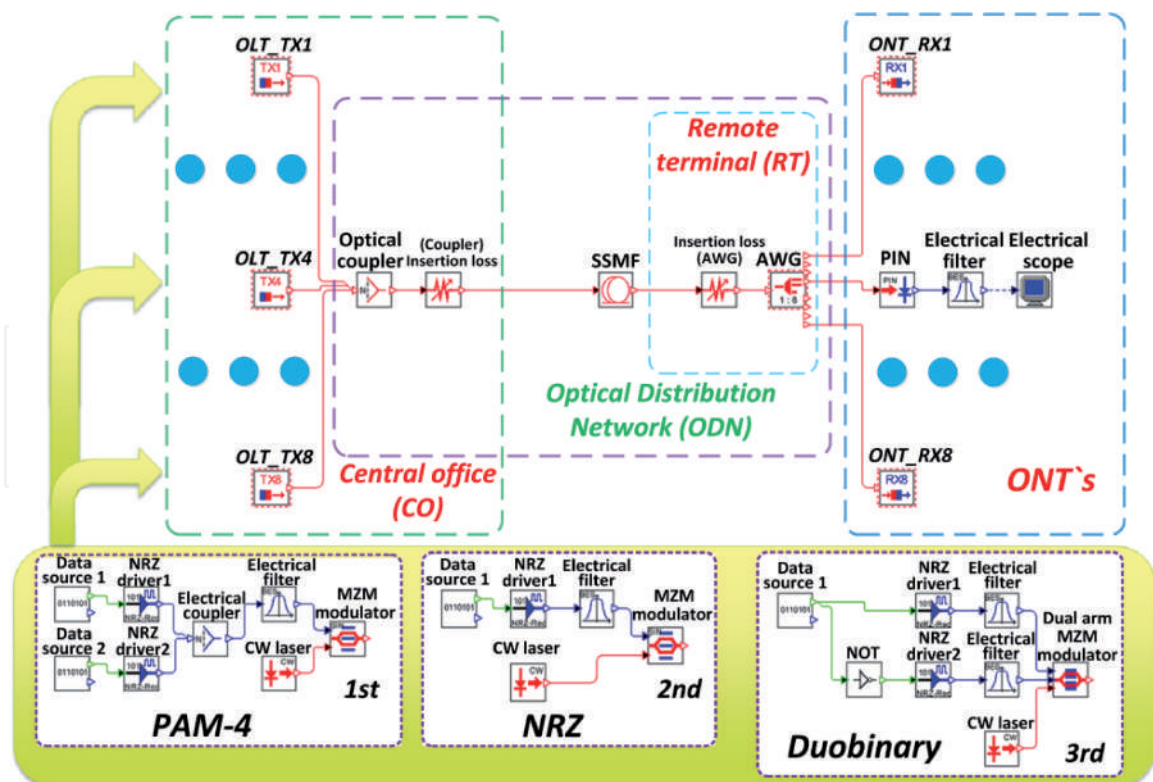


Figure 12.

Simulation scheme of 8-channel 20 Gbit/s transmission speed per channel PAM-4, DB and NRZ modulated WDM-PON optical transmission system.

In first simulation model PAM-4 transmitter is designed like previously, from two 10 Gbit/s NRZ coded electrical data signals (where one of them has twice larger amplitude), by coupled together with electrical coupler. Coupled PAM-4 electrical signal filtered with electrical Bessel low-pass filter (3-dB bandwidth is 10 GHz) and send to external MZM [21].

Second simulation model duobinary transmitter was realized with 20 Gbit/s bit rate per channel. Data source element with pseudo random bit sequence (PRBS) has only one logical output, where the output signal is divided in two signals. One of those signals is inverted by logical NOT element. Afterwards each data signal sent to NRZ drivers and filtered by Bessel low-pass filters (3-dB bandwidth is 5 GHz). Each NRZ coded electrical signal is passed to inputs of dual-arm MZM, at the end forming the DB transmitter [27].

Third simulation model NRZ transmitter consists of one NRZ driver with electrical signal input of data source with PRBS sequence. Afterwards NRZ coded data signal are directly connected to MZM RF signal input.

Following fixed parameters of optical and electrical elements was used: continuous wavelength (CW) laser output power + 6 dBm, extinction ratio 20 dB and 3 dB insertion loss of MZM, ITU-T G.652 SSMF with dispersion coefficient 17 ps/(nm × km), dispersion slope 0.056 ps/nm² × km and 0.2 dB/km attenuation coefficient [28]. Bandwidth of electrical LPF filters has been adjusted for optimal performance of each modulation format and have not been changed during research.

Each receiver consists of 40 GHz PIN photodiode with sensitivity equal to -19 dBm at 10 Gbit/s reference bit rate, dark current of 10 nA and responsivity of 0.8 A/W [29]. An electrical LPF filter bandwidth was adopted at receiver side for more successful system performance depending on the used modulation format. During the simulations LPF bandwidth of 15 GHz was chosen for PAM-4 modulated signals, and 10 and 17 GHz for DB and NRZ modulated electrical signals.

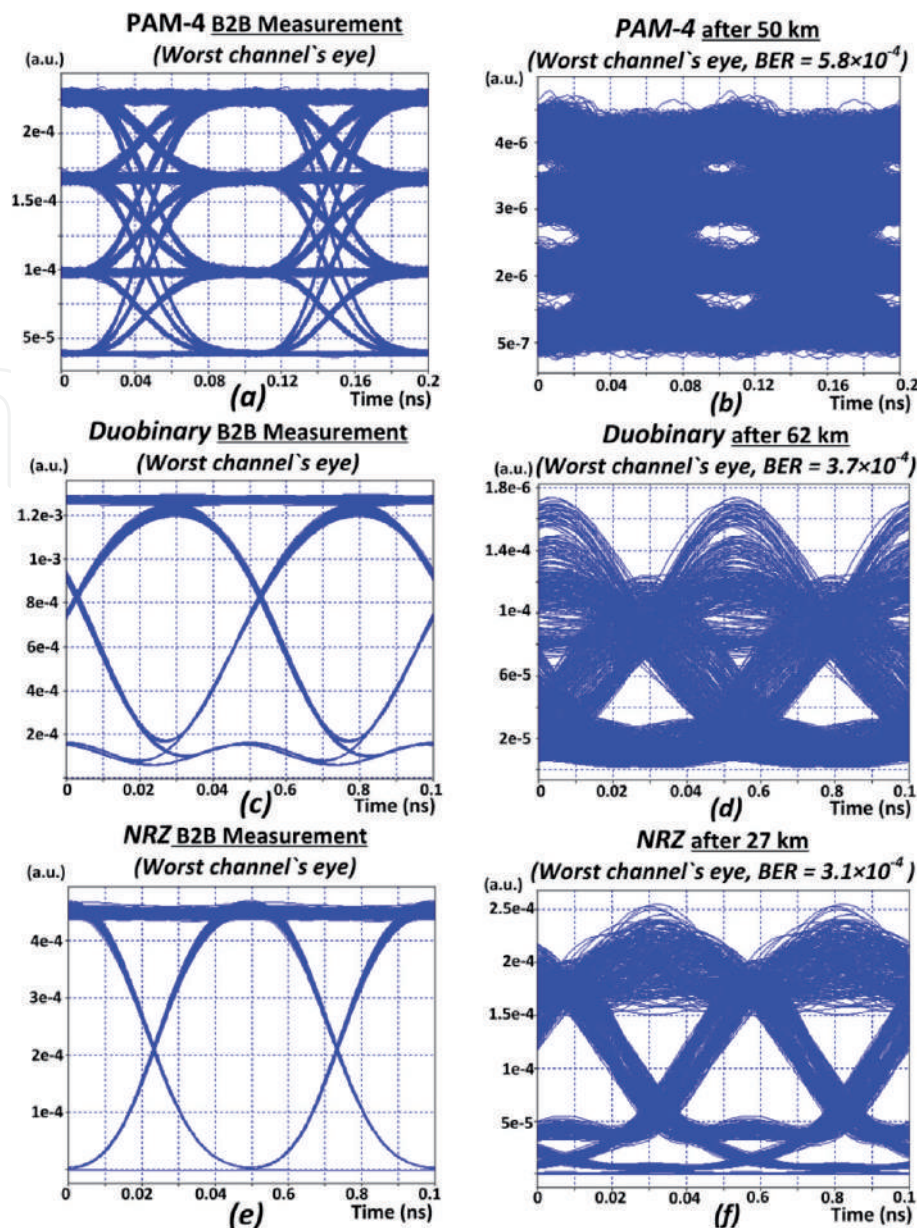


Figure 13.

Eye diagrams of received (a) PAM4, (c) DB and (e) NRZ signals after B2B transmission, and after maximal reached transmission distance: (b) 50 km with PAM-4, (d) 62 km with DB, (f) 27 km with NRZ modulated signals for 8-channel 20 Gbit/s per channel WDM -PON transmission system.

The BER threshold of 10^{-3} with additional FEC was used for our investigated WDM-PON transmission system to compare performance in terms of maximal network reach for PAM-4, DB, NRZ modulated optical signals. During the simulations it was observed that maximal achievable distance has minimal crosstalk impact on BER for all modulation formats, which was negligible, depending on our chosen channel spacing.

As it is shown in **Figure 13(a, c and e)** in B2B configuration for narrowest investigated 50 GHz channel spacing, the signal quality is good, eye is open and error-free transmission can be provided. After transmission the BER of received DB modulated signal with maximum reached distance of 62 km was 3.7×10^{-4} . PAM-4 and NRZ modulated signals shows 50 km and 27 km maximal reached transmission distance, where BER of received signal was 5.8×10^{-4} and 3.1×10^{-4} , please see **Figure 13(b, d and f)**. The largest network reach with BER below defined threshold, was provided by DB modulation format, extending the reach of 62 km.

5. Conclusions

Nowadays the WDM-PON systems rely on fixed wavelength transmitters and are expected to become more cost-efficient at high per user data rates. It was examined that different types of optical modulation formats are available for passive WDM fiber optical access networks. Implementation and research of multilevel modulation formats like PAM-4 and duobinary can dramatically improve the spectral efficiency and available bitrate by using the bandwidth of already existing optical, electro-optical or electrical devices. Theoretical simulations and experimental research methods showed possibility to double the available transmission speed in optical access networks by using the same bandwidth, e.g., instead of 10 Gbit/s transmit 20 Gbit/s signal by using 10 GHz electrical and electro-optical equipment, if PAM-4 modulation method is used. In our research we investigated existing optical modulation formats—widely used NRZ, DB and PAM-4 for optical access networks, by experimentally demonstrating and modeling system transmission in RSOFT OptSim simulation environment and Matlab software. As it shown by simulation results, narrowest channel spacing provides higher spectral efficiency. However, better signal quality and system performance are achieved with larger channel spacing interval, e.g., 100 GHz, mainly due to crosstalk between channels. From experimental data we can clearly see that the chromatic dispersion limits transmission capacity when bit rates increase. Implementation of the efficient compensation solution may sufficiently extend the reach of optical link and improve the transmission quality in our investigated WDM-PON systems.

Acknowledgements

This work has been supported by the European Regional Development Fund within the Activity 1.1.1.2 “Post-doctoral Research Aid” of the Specific Aid Objective 1.1.1 “To increase the research and innovative capacity of scientific institutions of Latvia and the ability to attract external financing, investing in human resources and infrastructure” of the Operational Programme “Growth and Employment” (No. 1.1.1.2/VIAA/1/16/044).

Author details

Toms Salgals*, Inna Kurbatska, Sandis Spolitis, Vjaceslavs Bobrovs
and Girts Ivanovs
Institute of Telecommunications, Riga Technical University, Riga, Latvia

*Address all correspondence to: toms.salgals@rtu.lv

IntechOpen

© 2019 The Author(s). Licensee IntechOpen. This chapter is distributed under the terms of the Creative Commons Attribution License (<http://creativecommons.org/licenses/by/3.0>), which permits unrestricted use, distribution, and reproduction in any medium, provided the original work is properly cited. 

References

- [1] Wei JL, Grobe K, Griesser H. High speed next generation passive optical networks: Performance, cost, and power dissipation. In: 2016 Progress in Electromagnetic Research Symposium (PIERS), Shanghai, China. 2016. pp. 4856-4857
- [2] Reed GT, Mashanovich G, Gardes FY, Thomson DJ. Silicon optical modulators. *Nature Photonics*. 2010;**4**(8):518-526
- [3] Nazemi A, Kangmin H, Catli B, DeLong C, Singh U, He T, et al. A 36Gb/s PAM4 transmitter using an 8b 18GS/s DAC in 28 nm CMOS. In: ISSCC 2005 IEEE International Digest of Technical Papers Solid-State Circuits Conference. 2015. pp. 1-3
- [4] Amirkhany A, Abbasfar A, Savoj J, Jeeradit M, Garlepp B, Kollipara RT, et al. A 24 Gb/s software programmable analog multi-tone transmitter. *IEEE Journal of Solid-State Circuits*. 2008;**43**(4):999-1009
- [5] Xiong C, Douglas MG, Jonathan EP, Jason SO, Wilfried H, William MJG. Monolithic 56 Gb/s silicon photonic pulse-amplitude modulation transmitter. *Optica*. 2016;**3**:1060-1065
- [6] Geisler DJ, Fontaine NK, Scott RP, He T, Paraschis L, Gerstel O, et al. Bandwidth scalable, coherent transmitter based on parallel synthesis of multiple spectral slices. In: Optical Fiber Communication Conference and Exposition (OFC/NFOEC), 2011 and the National Fiber Optic Engineers Conference. Los Angeles, CA; 2011, paper OTuE3. pp. 1-3
- [7] Spolitis S, Olmos JJ, Bobrovs V, Ivanovs G, Monroy I. A novel approach for transmission of 56 Gbit/s NRZ signal in access network using spectrum slicing technique. In: Asia Communications and Photonics Conference 2013: Conference Proceedings, China, Beijing. 12-15 December 2013, paper AF4D.2. pp. 1-3
- [8] Wagner C, Spolitis S, Olmos J, Bobrovs V, Tafur MI. Re-use of low bandwidth equipment for high bit rate transmission using signal slicing technique. In: Conference proceedings of Asia Communications and Photonics Conference, China, Hong Kong, 19-23 November 2015. Honkonga: Optical Society of America; 2015. pp. 1-3
- [9] Spolitis S, Wagner C, Olmos J, Bobrovs V, Ivanovs G, Monroy I. Experimental Demonstration of a Scalable Sliceable Transceiver for Optical Access Networks. In: Asia Communications and Photonics Conference 2014: Conference Proceedings, China, Shanghai, 11-14 November 2014. Shanghai: Optical Society of America; 2014. pp. 1-3
- [10] Keysight Technologies, Canada Keysight High Speed Digital Seminar Series. PAM-4 Stressed Pattern Generation. 2015. p. 41. Available from: http://www.keysight.com/upload/cmc_upload/All/HSDSeminarPaper4.pdf
- [11] Keysight Technologies. PAM-4 Design Challenges and the Implications on Test. Application Note. 2015. p. 12. Available from: <http://literature.cdn.keysight.com/litweb/pdf/5992-0527EN.pdf>
- [12] Kaur R, Dewra S. Duobinary modulation format for optical system—A review. *International Journal of Advanced Research in Electrical, Electronics and Instrumentation Engineering*. 2014;**3**:11039-11046. Available from: http://www.ijareeie.com/upload/2014/august/12_%20Duobinary.pdf
- [13] Qamar F, Khawar Islam M, Shah SZA, Farhan R, Ali M. Secure duobinary signal transmission in optical communication networks for high performance & reliability. *IEEE Access*. 2017;**5**:17795-17802

- [14] Kani J, Bourgart F, Cui A, Rafel A, Campbell M, Davey R, et al. Next-generation PON-part I: Technology roadmap and general requirements. *IEEE Communications Magazine*. 2009;47(11):43-49
- [15] Sanchez RJ, Hernandez A, Larrabeiti D. Troubleshooting PON networks effectively with carrier-grade ethernet and WDM-PON. *IEEE Communications Magazine*. 2014;52(2):7-13. Available from: <https://ieeexplore-ieee-org.resursi.rtu.lv/stamp/stamp.jsp?tp=&arnumber=6736739>
- [16] Bobrovs V. Analyzing and evaluation of channel interval in wavelength division multiplexing transmission systems [PhD thesis]. Riga: Riga Technical University; 2010. pp. 17-18
- [17] ITU-T G.694.1 Spectral Grids for WDM Applications: DWDM Frequency Grid. 2012. pp. 1-7
- [18] Olonkins S, Spolitis S, Lyashuk I, Bobrovs V. Cost effective WDM-AON with multicarrier source based on dual-pump FOPA. In: *International Congress on Ultra Modern Telecommunications and Control Systems and Workshops*, 2015. 2015. Art. No. 7002073. pp. 23-28
- [19] Spolitis S, Bobrovs V, Ivanovs G. Reach improvement of spectrum-sliced dense WDM-PON system. In: *Proceedings—2012 7th International Conference on Broadband, Wireless Computing, Communication and Applications, BWCCA 2012*. 2012. pp. 296-301. Art. No. 6363072
- [20] Anritsu. Enabling Precision EYE Pattern Analysis Extinction Ratio, Jitter, Mask Margin. pp. 3-6. Available from: https://dl.cdn-anritsu.com/en-us/test-measurement/files/Technical-Notes/Technical-Note/MP2100A_EE1100.pdf
- [21] Brunina D, Porto S, Jain A, Lai CP, Antony C, Pavarelli N, et al. Analysis of forward error correction in the upstream channel of 10Gb/s optically amplified TDM-PONs. In: *2015 Optical Fiber Communications Conference and Exhibition (OFC)*, Los Angeles, CA. 2015. pp. 1-3
- [22] ITU-T Recommendation G.984.2, Gigabit-capable Passive Optical Networks (GPON): Physical Media Dependent (PMD) layer specification. 2011, 1-36. Available from: https://www.google.com/url?sa=t&rct=j&q=&esrc=s&source=web&cd=2&ved=2ahUKEwigteS7mMXgAhVl6KYKHU1UD6EQFjABegQICRAC&url=https%3A%2F%2Fwww.itu.int%2Frec%2Fdoclog_in_pub.asp%3Flang%3De%26id%3DT-REC-G.984.2-200303-I!!PDF-E%26type%3Ditems&usg=AOvVaw2nWcdEiNYzk3CnHZJ8tPgR
- [23] Salgals T, Spolitis S, Olonkins S, Bobrovs V. Investigation of 4-PAM modulation format for use in WDM-PON optical access systems. In: *Progress in Electromagnetics Research Symposium (PIERS 2017)*, St. Petersburg, Russia. 2017. pp. 1-4
- [24] Forzati M, Berntson A, Martensson J, Pincemin E, Gavignet P. NRZ-OOK transmission of 16 × 40 Gb/s over 2800 km SSMF using asynchronous phase modulation. In: *IEEE Conference on Lasers and Electro-Optics and 2008 Conference on Quantum Electronics and Laser Science*. 2008. pp. 1-2
- [25] Wang Y, Gai W, Tang L. A novel 40-Gb/S PAM4 transmitter with power-efficient pre-emphasis. In: *IEEE International Conference on Solid-State and Integrated Circuit Technology (ICSICT)*. 2014. pp. 1-3
- [26] Salgals T, Skladova L, Vilcane K, Braunfelds J, Spolitis S. Evaluation of 4-PAM, NRZ and duobinary modulation formats performance for use in 20 Gbit/s DWDM-PON optical access systems. In: *2018 Advances in Wireless and Optical Communications*

(RTUWO 2018): Proceedings, Latvia,
Riga. 15-16 November 2018

[27] Kurbatska I, Spolitis S, Bobrovs V,
Alševska A, Ivanovs Ģ. Performance
comparison of modulation formats
for 10 Gbit/s WDM-PON systems. In:
2016 Advances in Wireless and Optical
Communications (RTUWO 2016):
Proceedings, Latvia, Riga, 3-4 November
2016. Piscataway: IEEE; 2016. pp. 51-54

[28] ID Photonics GmbH. CoBrite DX1–
Laser. Technical Specification. 2017.
pp. 1-4. Available from: [https://www.
id-photonics.com/images/stories/PDF/
Data_sheet_CBDX1-x-x-xx.pdf](https://www.id-photonics.com/images/stories/PDF/Data_sheet_CBDX1-x-x-xx.pdf)

[29] Optilab Technical Specification
of “40 GHz Linear InGaAs PIN
Photodetector”. 2016. pp. 1-4. Available
from: [https://www.oequest.com/
getDatasheet/id/9716-9716.pdf](https://www.oequest.com/getDatasheet/id/9716-9716.pdf)

IntechOpen

Mitigating Turbulence-Induced Fading in Coherent FSO Links: An Adaptive Space-Time Code Approach

*Ojo O. Adedayo, Oluwafemi B. Ilesanmi,
Ogunlade M. Adegoke and Ajibade Adedayo*

Abstract

Free space optical communication systems have witnessed a significant rise in attention over the last half a decade owing largely to their enormous bandwidth and relative ease of deployment. Generally, free space optical communication systems differ in their detection mechanism as various detection mechanisms are being reported, including intensity modulation/direct detection FSO, differential FSO and coherent FSO. In this chapter, we explore the prospect of obtaining an optimally performing FSO system by harnessing the cutting-edge features of coherent FSO systems and the coding gain and diversity advantage offered by a four-state space-time trellis code (STTC) in order to combat turbulence-induced fading which has thus far beleaguered the performance of FSO systems. The initial outcomes of this technique are promising as a model for various visible light communication applications.

Keywords: free space optical communication, space-time trellis code, turbulence, coherent detection

1. Introduction

Telecommunication is one of the most important innovations in the history of mankind as it affords people the opportunity to communicate rapidly and reliably over long distances, often breaking physical and geographical barriers to make the world a global village as it is known today. One of the key ingredients in the heart of communication technologies over the last century is wireless communication. The advent of RF wireless communication techniques and protocols has been instrumental to the giant strides made in the communication domain as it eliminates the cumbersome requirement of lengthy wired connections, a requirement which has often been a great limitation for wired communication systems.

RF wireless communication systems enjoyed significant attention and penetration but soon became a victim of its success as more and more contents are demanded by users due to the proliferation of data, video, gaming and general broadband multimedia. These demands have prompted communication system engineers to explore

more efficient, faster and reliable wireless communication techniques. To this end, free space optical (FSO) communication has been a viable solution [1].

Free space optical communication is a communication technology that employs light as carrier by modulating baseband information with optical carriers often from laser beams through free space to the receiver [2]. The path of connection between FSO transmitters and the receivers are known as FSO links. Even though the very first optical system dates back to the eighteenth century, modern FSO communication systems were first widely deployed by the National Aeronautics and Space Administration (NASA) and have since become a promising broadband wireless access technology. FSO communication systems are also being combined with standard RF systems in order to form hybrid communication systems that harness the unique features of RF and FSO communication systems to enhance performance, capacity and reliability.

Characteristically, FSO communication systems are highly secure as they have high immunity to interference with the use of secure point-to-point line-of-sight links, they require no licensing or regulatory permission, and they are fast and can be easily deployed and operated compared to other systems like the fiber optic systems [3]. These features make FSO communication the favored option for the provision of high-speed links for a variety of next generation optical applications including broadcast, security, wireless backhaul at a data rate as high as 40 Gbps [4], fiber backup and last mile communication [5]. Finally, the ease of setup and cost effectiveness of FSO systems have made them the preferred option for restoring connection in case of disaster.

However, the performance of FSO communication systems are greatly affected by turbulence-induced fading [6–12], and different investigations are currently being explored to address this challenge. The inhomogeneity of the temperature and pressure of the atmosphere causes local variations in the refractive index as light propagates from the transmitter to the photoreceptor; these variations degrade the performance of FSO links significantly.

Geared towards the improvement of the performance of coherent FSO communication systems in the presence of atmospheric turbulence, this work examines the error reduction schemes currently being employed for FSO links and presents an adaptive space-time trellis code (STTC) scheme for coherent FSO links.

2. Free space optical communication: types and variants

In terms of reception technique, however, the most commonly reported variants of FSO communication systems are the direct detection/intensity modulated (IM/DD) FSO system and the coherent FSO system. The IM/DD FSO communication systems convey the information to be transmitted only on the intensity of the emitted light, and the receivers simply decode the information as the light changes in intensity. In coherent FSO communication systems, however, other signal properties such as phase and frequency may be employed in conveying the information. At the receiving end, as against simply observing changes in light intensity as in the case of IM/DD FSO systems, coherent FSO communication systems, first, mix the received field optically with a local oscillator before the actual photodetection. So far, more works on the IM/DD FSO communication system are being reported in literature owing to its simplicity of detection as less complex receivers and algorithms are required. Coherent FSO systems, though more complex, however, offer superior performance in terms of improved receiver sensitivity and background noise rejection [13].

Finally, in terms of communication range, FSO communication systems can be characterized into short-range, medium-range, long-range and inter-terrestrial FSO

systems depending on the application for which they are deployed, and these applications include inter-chip communication, inter-vehicular communication, metropolitan area communication as well as satellite and space exploration.

3. FSO system and channel models

Concerted efforts being expended by researchers in the quest of effectively modeling the FSO channel are geared towards understanding the channel and serving as the template upon which FSO modulators, demodulators, receivers and other devices can work. Accurate mathematical models for FSO communication system are the basis upon which the development of high-performing hardware is established, despite huge technical challenge of turbulence-induced fading. This challenge is however being addressed using various techniques as summarized in **Figure 1**.

In the wavelength diversity schemes, the source information is encoded into different wavelengths obtainable from different constituents of the infrared spectrum.

4. Turbulence models

One of the most crucial steps in the attempts to mitigate the degradation in the performance of optical communication systems is accurate modeling of the atmospheric turbulence under different conditions. Below are some of the irradiance functions presented in terms of probability distribution functions.

4.1 Lognormal distribution

The lognormal distribution is one of the most widely employed for weak atmospheric turbulence distribution. Here, the irradiance value received at the receiver follows the distribution [9]

$$f_A(a) = \frac{1}{2a(2\pi\sigma_x^2)^{\frac{1}{2}}} \exp\left(-\frac{(\ln a + 2\sigma_x)^2}{8\sigma_x^2}\right) \quad (1)$$

where μ_x is the mean value of fading and σ_x^2 is the fading covariance.

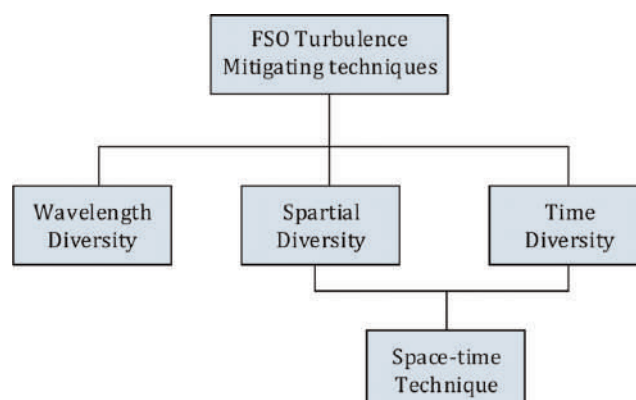


Figure 1.
 Some turbulence mitigation techniques in FSO systems.

4.2 K-distribution

The K-distribution turbulence model is often used to describe strong atmospheric turbulence conditions (non-Rayleigh sea clutter). For K-distribution atmospheric turbulence model, the probability distribution function $p(I)$ is expressed as [14]

$$p(I) = \frac{2\alpha}{\Gamma(\alpha)} (\alpha I)^{\frac{\alpha-1}{2}} K_{\alpha-1}(2\sqrt{\alpha I}), I > 0, \alpha > 0 \quad (2)$$

$K_m(\bullet)$ = modified Bessel function of second kind and order m .

4.3 Negative exponential distribution

Negative exponential turbulence model is employed for saturated turbulence cases where the probability distribution function of the received irradiance value is expressed as [15]

$$p(I) = \frac{1}{I_0} \exp\left(\frac{-I}{I_0}\right), I_0 > 0 \quad (3)$$

where I_0 denotes the mean irradiance.

4.4 Gamma-gamma distribution

The gamma-gamma model is very commonly used in FSO communication literatures because it is applicable for a wider range of turbulence conditions. In comparison with measured data, gamma-gamma distribution is effective in describing weak to strong atmospheric turbulence conditions. The PDF is expressed as [16]

$$f_{\tilde{H}}^{GG}(h) = \frac{2(\alpha\beta)^{\frac{\alpha+\beta}{2}}}{\Gamma(\alpha)\Gamma(\beta)} h^{\frac{\alpha+\beta}{2}-1} K_{\alpha-\beta}(2\sqrt{\alpha\beta h}) \quad (4)$$

where $K_\nu(x)$ is the modified Bessel function of the second kind and α and β are the turbulence parameter.

5. Space-time trellis coded coherent FSO

The essence of space-time trellis encoder is to employ mapping functions which are representatives of their trellis diagrams to map binary data to modulation symbols. We design and evaluate the performance of space-time trellis code with two transmit antennas for FSO channel. In order to simplify the design and yet ensuring that there is no jeopardy to the intended MIMO configuration, we represent, for the two transmit antennas, the input bitstream c as [17]

$$c = (c_0, c_1, c_2, \dots, c_t, \dots) \quad (5)$$

where c_t , at any instant t denotes a group of two information bits expressed as

$$c_1 = (c_t^1, c_t^2) \quad (6)$$

As shown in **Figure 2**, the encoder, made up of feedforward shift registers, converts the input bit sequence into a sequence of modulated signals

$x_0, x_1, x_2, \dots, x_t, \dots$, where each element x_t of this sequence is the space-time symbol at a given time t .

The output x_t^i of the encoder for the i th transmitter at time t is expressed as [19]

$$x_t^i = \sum_{k=1}^m \sum_{j=0}^{v_k} g_{j,i}^k c_{t-j}^k \text{Mod } 2, i = 1, 2 \quad (7)$$

Space-time code (STC) leverages on the features of both time diversity and space diversity to combat turbulence-induced fading in wireless communication systems. RF wireless systems in particular have witness an explosion of interest in the use of space-time coding to improve communication system performance in terms of error control and turbulence mitigation, and FSO communication systems are also witnessing a lot of interest in using this same tool for similar purpose.

In this chapter, we present an adaptive four-state space-time trellis coded coherent FSO system with two transmit lasers, as illustrated in **Figure 3**. Firstly, the error correction performance of the system is complemented by the interleaver, a mechanism put in place to distribute the burst errors—an effect of deep fade, onto different codeword lengths.

Denoting the average SNR as γ , we take the received signal matrix for each codeword C as [20]

$$R = \sqrt{\gamma}CH + Z \quad (8)$$

where H and Z are the channels and noise matrices, respectively, and H is modeled in terms of the uniformly distributed channel gain phase $\phi_{\mu\nu}$ and the channel gain amplitude $a_{\mu\nu}$ as [20]

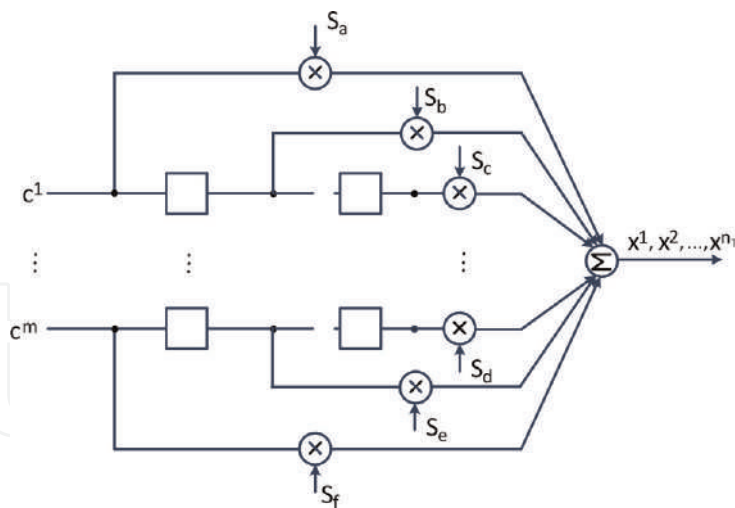


Figure 2.
 STTC encoder [18].

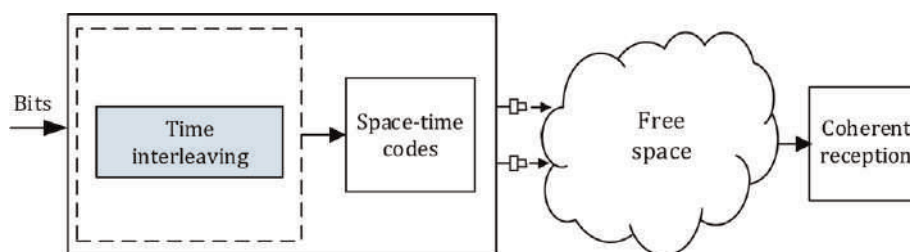


Figure 3.
 Space-time trellis coded FSO communication system.

$$[H]_{\mu\nu} = a_{\mu\nu} e^{j\phi_{\mu\nu}} \quad 1 \leq \mu \leq 2, 1 \leq \nu \leq N \quad (9)$$

We begin our analysis using the pairwise error probability (PEP), which is the probability that the decoder erroneously decodes a transmitted STTC codeword \mathbf{C} as $\mathbf{C}' = [c'_0 \dots c'_{T-1}]$. Then, assuming a gamma-gamma fading distribution as portrayed in Eq. (4), we represent the conditional PEP as [5]

$$P_e(E|H) = Q\left(\sqrt{\frac{\gamma d^2(E)}{2}}\right) \quad (10)$$

where

$$d^2(E) = \text{tr}\{H^H E^H E H\} \quad (11)$$

Now, writing a matrix B and its constituent elements as

$$B = \begin{bmatrix} b_{11} & b_{12} \\ b_{12}^* & b_{22} \end{bmatrix} \quad (12)$$

and by equating B with the positive semi-definite matrix $E^H E$ and comparing the elements thereof, where E represents the error matrix in the decoding of the codewords and $(\bullet)^H$ denotes the Hermitian transpose function, we write the asymptotic pairwise error probability of the systems as [21]

$$PEP = \frac{(\pi a_h^2 \Gamma^2(2\mu) F(\mu, \mu; 1; \xi^2))^N \Gamma(2\mu N + \frac{1}{2}) \gamma^{-2\mu N}}{2\sqrt{\pi} (b_{11} b_{22}) \mu^N \Gamma(2\mu N + 1) \Gamma^{2N}(\mu + \frac{1}{2})} \quad (13)$$

where the Gaussian hypergeometric function $F(\bullet)$ is readily computed by using specialized computing functions from libraries of most engineering computing applications or by using fast-converging series [20] as

$$F\left(\frac{t}{2}, \frac{t}{2}; 1; \xi^2\right) = \sum_{n=0}^{\infty} \left[\binom{\frac{t}{2} + n - 1}{n} \xi^{2n} \right]^2 \quad (14)$$

The function Γ in Eq. (13) is a function of the channel parameters α and β ; these parameters may be obtained through the Rytov variance, which in turn is a function of the refractive index, the transmission path length between the transmitter and the receiver and the optical wave number [22].

With proper modifications of the values of ξ , Eq. (13) and by extension, Eq. (14), could be modified for general case as well as specific non-orthogonal space-time codes for coherent free space optical communication system. We leverage onto this feature to introduce an adaptive orthogonality controller which adjusts its parameters to any STC supplied thereby not merely eliminating the orthogonality condition as presented in [21] but effectively introduces additional flexibility to the coding scheme.

Readers are to note, however, that several space-time code designs reported for IM/DD FSO communication systems cannot be simply employed for coherent FSO communication systems. This caveat is due to the peculiarities inherent in coherent FSO systems. In addition to this, it should also be noted that in this work, it is assumed that the transmit lasers simultaneously illuminate the receivers with the receivers far away enough from the transmit lasers to assume independent and identically distributed (iid) fading gain.

6. Results and discussion

In this section, the results of the space-time code technique for mitigating turbulence-induced fading in coherent FSO communication systems are presented. Free space optical systems often face the challenge of fading as well as pointing error, and the effect of the latter has been well addressed [23]. The performance of the link under gamma-gamma turbulence is investigated for two transmit lasers, first, with two receivers and then four and six receivers, respectively, as shown in **Figure 4**. Apart from the reduction of the average bit error rate with increase in SNR values, the result shows that at low average SNR, the average performance of the link under the turbulence condition for the different number of receivers are relatively close. However, the difference in performance becomes apparent at higher SNRs as evidenced from SNR 20 to SNR 38.

Although gamma-gamma distribution have been well reported as suitable for modeling weak turbulence as well as strong turbulence scenarios, for the sake of analysis, we employ the values $\alpha = 3.0$ and $\beta = 2.7$. The choice of these values is

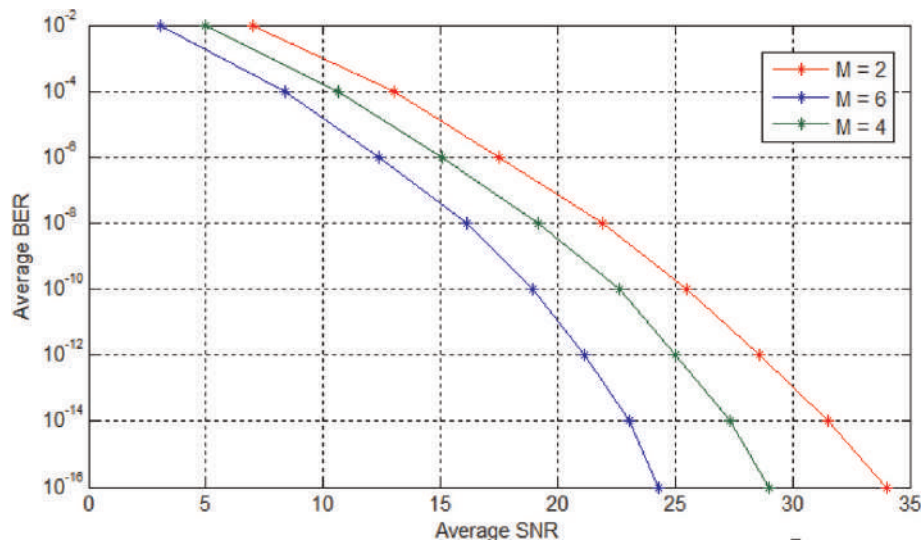


Figure 4.
 Performance of coherent FSO link with different receivers.

Coding scheme	Modulation scheme	Detection type	SNR (dB)	References
STBC	OOK	IM/DD	—	[24]
STC variant—no additional constellation extension	PPM	IM/DD	$0 \leq \text{SNR} \leq 30$	[25]
STBC	OOK	IM/DD with maximum likelihood (ML)	—	[26]
Alamouti-type STC	OOK and PPM	Coherent detection and IM/DD	Additional 3 dB loss relative to BPSK	[27]
STTC	—	IM/DD	$0 \leq \text{SNR} \leq 90$	[28]
Extended Alamouti STC with turbo coding	PPM	IM/DD	$0 \leq \text{SNR per bit} \leq 30$	[29]
STTC	QPSK	Coherent detection	$0 \leq \text{SNR} \leq 35$	This work

Table 1.
 Some coding schemes employed for FSO links.

informed by their popularity in literature as the performance of this work is compared with earlier works in this domain, many of which employed the gamma-gamma distribution parameter above.

FSO communication systems vary in their reception mechanisms as well as modulation techniques. Many works have employed OOK, PPM and QPSK or a combination of these modulation schemes all in a bid to mitigate turbulence-induced fading in FSO links. A few of these works and their corresponding features in comparison to this work are presented in **Table 1**.

Even though the efficiency of space-time codes for turbulence mitigation or error correction in intensity modulated/direct detection FSO systems remains inconclusive in literature, we establish that space-time coding—adaptive space-time trellis codes as in the case of this work, together with inherent potentials of coherent reception for FSO systems—remains a promising solution for free space optical communication systems.

7. Conclusion

For coherent free space optical communication links, we explore the space-time approach to mitigating turbulence-induced fading which thus far remains a serious performance degrading factor for FSO systems. Additionally, as an effort geared towards realizing the promising potentials of coherent free space optical communication systems, we propose an adaptive orthogonality controller for seamless deployment of space-time codes for coherent free space optical communication systems.

Author details

Ojo O. Adedayo^{1*}, Oluwafemi B. Ilesanmi², Ogunlade M. Adegoke¹
and Ajibade Adedayo¹

¹ Department of Electrical Electronic and Computer Engineering, College of Engineering, Afe Babalola University Ado-Ekiti (ABUAD), Ado-Ekiti, Ekiti State, Nigeria

² Department of Electrical Electronic Engineering, Faculty of Engineering, Centre for Research in Electrical Communication (CRECO), Ekiti State University, Ado-Ekiti, Ekiti State, Nigeria

*Address all correspondence to: ojoao@abuad.edu.ng

IntechOpen

© 2019 The Author(s). Licensee IntechOpen. This chapter is distributed under the terms of the Creative Commons Attribution License (<http://creativecommons.org/licenses/by/3.0>), which permits unrestricted use, distribution, and reproduction in any medium, provided the original work is properly cited. 

References

- [1] Adedayo O, Oluwafemi I, Esan O. Space-time codes in free space optical communications: A case for improved spectral efficiency. *The International Journal of Microwave and Optical Technology*. 2018;**13**(4):359-368
- [2] Kaur G, Singh H, Sappal AS. Free space optical using different modulation techniques—A review. *International Journal of Engineering Trends and Technology (IJETT)*. 2017;**43**(2): 109-115
- [3] Mahdieh MHÃ, Pournoury M. Optics & laser technology atmospheric turbulence and numerical evaluation of bit error rate (BER) in free-space communication. *Optics and Laser Technology*. 2010;**42**(1):55-60
- [4] Leitgeb E, Sheikh S, Chlestil C, Gebhart M, Birnbacher U. Reliability of FSO links in next generation optical networks. *IEEE ICTCON*. 2005:394-401
- [5] Garcia-Zambrana A, Castillo-vazquez C, Castillo-vazquez B. Space-time trellis coding with transmit laser selection for FSO links over strong atmospheric turbulence channels. *Optics Express*. 2010;**18**(6):1293-1300
- [6] Tang X, Xu Z. Outage probability of multihop free space optical communications over Nakagami fading channels. 2013. pp. 199–202
- [7] Bayaki E, Schober R, Mallik RK. Performance analysis of MIMO free-space optical systems in gamma-gamma fading. *IEEE Transactions on Communications*. 2009;**57**(11)
- [8] Ninos MP, Nistazakis HE, Tombras GS. On the BER performance of FSO links with multiple receivers and spatial jitter over gamma-gamma or exponential turbulence channels. *Optik—International Journal for Light and Electron Optics*. 2017:1-28
- [9] Alimi I, Shahpari A, Sousa A, Ferreira R, Monteiro P, Teixeira A. Challenges and opportunities of optical wireless communication technologies. In: *Optical Communication Technology*, Pedro Pinho, IntechOpen; 2017
- [10] Abou-rjeily C, Member S. Performance analysis of FSO communications with diversity methods: Add more relays or more apertures? *IEEE Journal on Selected Areas in Communications*. 2015;**33**(9): 1890-1902
- [11] Ogunmodede HA, Afullo TJ, Owolawi PA. Performance evaluation of OFDM-FSO communication systems using-QAM and BPSK modulation under log-normal channel. In: *The Southern Africa Telecommunication Network and Application Conference*; 2016. pp. 98-103
- [12] Niu M, Cheng J, Holzman JF. Space-time coded MPSK coherent MIMO FSO systems in gamma-gamma turbulence. In: *IEEE Wireless Communications and Networking Conference (WCNC)*; 2013. pp. 4266-4271
- [13] Kumar P. Comparative analysis of BER performance for direct detection and coherent detection FSO communication systems. In: *Fifth International on Communication Systems and Network Technologies*; 2015. pp. 369-374
- [14] Khalighi MA, Uysal M. Survey on free space optical communication: A communication theory perspective. *IEEE Communication Surveys and Tutorials*. 2014;**16**(4):2231-2258
- [15] Anbarasi K, Hemanth C, Sangeetha RG. A review on channel models in free space optical communication systems. *Optics and Laser Technology*. 2017;**97**: 161-171

- [16] Letzepis N, Guillén A. Outage probability of the Gaussian MIMO free-space optical channel with PPM. *IEEE Transactions on Communications*. 2009; **57**(12):3682-3690
- [17] Rana SM, Alam SMS, Fatema KJ. Code construction and performance evaluation of space time trellis code (STTC) over Rayleigh fading channel. In: *Proceedings of the 14th International Conference on Computer and Information Science and Technology*; 2011. pp. 22-24
- [18] Li Y, Ge Y, Yu J, Dai J, Fu X, Yang E. Improved space-time trellis coded OFDM scheme for frequency selective fading channels. *IEEE Canadian Conference on Electrical and Computer Engineering*. 2004:1967-1970
- [19] Vucetic B, Yuan J. *Space-Time Coding*. West Sussex, England: John Wiley & Sons Ltd; 2003
- [20] Nezampour A, Schober R. Asymptotic analysis of space-time codes in generalized fading channels. *IEEE Communications Letters*. 2009;**13**(8): 561-563
- [21] Bayaki E, Schober R. Performance and design of coherent and differential space-time coded FSO systems. *Journal of Lightwave Technology*. 2012;**30**(11): 1569-1577
- [22] Niu M, Cheng J, Holzman JF. Terrestrial coherent free-space optical communication systems. In: *Optical Communication*. British Columbia, Canada: The University of British Columbia (UBC); 2012. pp. 169-176
- [23] Dubey V, Chandra V. Effect of pointing error on cooperative free space optical communication systems under different channel conditions. In: *International Conference on Advanced Networks and Telecommunications System (ANTS)*; 2015. pp. 2-5
- [24] Garcia-Zambrana A. Error rate performance for STBC in free-space optical communications through strong atmospheric turbulence. *IEEE Communications Letters*. 2007;**11**(5): 390-392
- [25] Abou-Rjeily C, Fawaz W. Space-time codes for MIMO ultra-wideband optical communications and MIMO free-space optical communications with PPM. *IEEE Journal on Selected Areas in Communications*. 2008;**26**(6):938-947
- [26] Wang K, Nirmalathas A, Lim C, Alameh K, Skafidas E. Space-time coded high-speed reconfigurable free-space card-to-card optical interconnects with extended range. *The Journal of the Optical Society of America*. 2016;**1**(16): 6-8
- [27] Abaza M, Mesleh R, Mansour A, Aggoune EM. Spatial diversity for FSO communication systems over atmospheric turbulence channels. In: *IEEE WCNC '14 Track 1: PHY and Fundamentals*. vol. 1. 2014. pp. 382-387
- [28] Mesleh R, Elgala H, Haas H. Optical spatial modulation. *Journal of Optical Communications and Networking*. 2011; **3**(3):234-244
- [29] Khare V, Chadha D. Extended alamouti space time coding scheme with turbo coding for free space optical communication. In: *International Conference on Computational Intelligence and Communication Networks*; 2011. pp. 366-369

Spatial Light Modulation as a Flexible Platform for Optical Systems

Cátia Pinho, Isiaka Alimi, Mário Lima, Paulo Monteiro and António Teixeira

Abstract

Spatial light modulation is a technology with a demonstrated wide range of applications, especially in optical systems. Among the various spatial light modulator (SLM) technologies, e.g., liquid crystal (LC), magneto-optic, deformable mirror, multiple quantum well, and acoustic-optic Bragg cells, the ones based on liquid crystal on silicon (LCoS) have been gaining importance and relevance in a plethora of optical contexts, namely, in telecom, metrology, optical storage, and microdisplays. Their implementation in telecom has enabled the development of high-capacity optical components in system functionalities as multiplexing/demultiplexing, switching and optical signal processing. This technology combines the unique light-modulating properties of LC with the high-performance silicon complementary metal oxide semiconductor properties. Different types of modulation, i.e., phase, amplitude or combination of the two, can be achieved. In this book chapter, we address the most relevant applications of phase-only LCoS SLM for optical telecom purposes and the employment of SLM technology in photonic integrated circuits (PICs) (e.g., field-programmable silicon photonic (SiP) circuits and integrated SLM application to create versatile reconfigurable elements). Furthermore, a new SLM-based flexible coupling platform with applications in spatial division multiplexing (SDM) systems (e.g., to efficiently excite different cores in MCF) and characterization/testing of photonic integrated processors will be described.

Keywords: spatial light modulator (SLM), liquid crystal silicon (LCoS) SLM, optical transforms, computer-generated holography (CGH), photonic integrated circuits (PICs), spatial division multiplexing (SDM)

1. Introduction

There has been significant growth in the required capacity of the telecommunication systems, which can be attributed to the proliferation of mobile devices, bandwidth-intensive applications, and services [1–3]. As a result, a significant increase in the broadband connections as well as the related multimedia traffic on a yearly basis [4–6] has been progressing. Moreover, the traffic explosion has been one of the challenges being faced in telecommunication systems [2, 7]. Also, it has been observed that the traditional electronic media which are based on copper are unable to meet the system requirements majorly in terms of bandwidth and latency [5, 8–10].

To address the challenges, optical fiber-based transport systems have been employed in different fields of communication systems as viable and reliable solutions. The widely employed optical transport systems are based on single-mode fiber (SMF). To enhance the capacity of single-core SMF, advanced modulation formats and wavelength division multiplexing (WDM) are normally employed. However, the growing demand for further video/image storage capacity and the increase in cloud service adoption, which is as a result of numerous smartphones and other Internet-based gadgets, have led to research on solutions for effective bandwidth optimization [11, 12]. This is due to the fact that the conventional SMF-based transport systems have been observed to be approaching Shannon's limit [13] and the achievable maximum capacity will not be sufficient to support the envisaged massive connection demanded by the next-generation networks [5, 14–16]. Besides the capacity that is expected to be saturated around 100 Tbit/s owing to the physical limits, the conventional SMF schemes with WDM might be unable to meet the power consumption, spatial efficiency, and cost requirements of the communication systems [16, 17].

There has been considerable attention on multicore fiber (MCF) as a feasible solution capable of addressing the capacity limit of a conventional SMF-based scheme [15, 18, 19]. For effective implementation of MCF, the research community has been working diligently on improved cost-efficient and scalable networking infrastructure solutions. A notable optical transport scheme that can exploit the space dimension in order to address the optical system capacity crunch and improve the system performance is spatial division multiplexing (SDM) [19]. Moreover, it has been observed that MCF is an efficient and main enabling technology for the SDM systems [16, 18]. Apart from the MCF, SDM implementation for multimode fiber (MMF) has also been attracting significant attention [17, 18]. Nevertheless, the MCF implementation is susceptible to and can be constrained by the transmission impairments such as nonlinearities and inter-core cross talk (XT) between signals at the neighboring cores that may be presented via multiple optical paths. This may have a significant effect on the system performance regarding the transmission range and the network size [16, 17]. Furthermore, the extent of the presented performance degradation by the transmission impairments varies with the MCF fiber types (i.e., 3-core, 7-core, 13-core, 19-core, 37-core, and 61-core) [16, 20]. A practical solution for addressing the MCF implementation challenges is spatial light modulation.

Spatial light modulators (SLM) can be employed for exciting different cores and/or modes in order to mitigate the transmission impairments introduced by multiple optical paths, as it enables arbitrary removal or addition of channels with the aid of software, i.e., implementation of a diffractive optical element by computer-generated holograms (CGH). Due to the SLM support for dynamic reconfiguration of optical wave fronts, it can be employed for core and mode multiplexing and demultiplexing [5, 21, 22]. In addition, the use of silicon photonic (SiP) onboard transceivers that are coupled on the MCF for supporting transmissions has been shown to be promising. This is due to the fact that there is no need for fan-in/fan-out or core pitch conversion devices that may give rise to further system complexity [16].

Optical communication evolution has brought about the emergence of improved photonic integrated circuits (PICs) that present economic and sustainable alternative to data transmission [9]. Therefore, it is expected to be an enabling technology, capable of contributing significantly in a number of fields [8]. As a result, various benefits are offered, such as small weight and volume, low power consumption, high mechanical and thermal stability, and the ease of assembling a number of complex systems.

PIC can be generally characterized as a multiport device with an integrated system of optical elements such as attenuators, modulators, multiplexers, detectors, lasers, and optical amplifiers that are embedded in a single chip using a waveguide (WG) architecture [23]. However, it has been observed that optical component testing is very challenging and time-consuming as well [24]. This can be attributed to the required tight three-dimensional (3D) alignment tolerances, to ensure accurate light coupling. Hence, with notable development and growing adoption of PIC in the communication networks, advanced methods are imperative for an accurate PIC performance testing as well as characterization. As aforementioned, based on the support for dynamic reconfiguration of light, SLM can be employed for optical PIC testing and characterization, by exploring this feature in the feeding and/or receiving the optical signal into the PIC [8, 23].

In this chapter, we focus on the most pertinent applications of phase-only liquid crystal on silicon (LCoS) SLM for optical telecom purposes and the employment of SLM technology in PIC, e.g., field-programmable silicon photonic circuits and integrated SLM application to create versatile reconfigurable elements. Furthermore, a new SLM-based flexible coupling platform for applications in SDM systems and characterization/testing of photonic processors will be presented.

In Section 2, SLM working principle and their applications in telecom are addressed in more detail. The applied methodology (i.e., algorithms and experimental setup) to create a diffraction optical element through the implementation and optimization of CGH is described in Section 3. In Section 4, discussion on the obtained results from the experimental implementation of CGH for SDM and PIC applications is presented. An overall conclusion regarding the employment of the SLM technology as a flexible platform for optical systems is provided in Section 5.

2. Spatial light modulator (SLM)

Optical signal processing has been providing relevant solutions to convert data into spatially modulated coherent optical signals with SLM devices, allowing the effective implementation of digital holograms [25]. One of the most useful properties of the hologram is its ability to control phase and amplitude of light in the far field. The Fourier transform describes the relationship between a hologram (near field) and its corresponding replay field (far field). The far field can be formed at the focal point of a positive lens or an infinite distance from the near field plane in free space [25, 26], as depicted in **Figure 1**.

Holograms can reproduce waveforms from an existing object. With digital advances and optical signal processing, it is possible to numerically calculate interference patterns to generate completely synthetic wave fronts of arbitrary form. These interference patterns can have different denominations, such as CGH, diffractive optical elements (DOE), phase/amplitude masks, diffractive grating, etc. [26]. All operate in the principle of diffraction, so it is somehow an arbitrary choice of terminology.

The SLM is a device that can be used to modulate light in accordance with a fixed spatial (pixel) pattern and can be programmed electrically. Usually, it can be exploited for incident light phase and/or amplitude control. Subsequently, phase-only, amplitude-only, or the combination of phase-amplitude can be readily realized with SLM. There are a number of modulation mechanisms that can be employed. One of the attractive and widely used ones is electro-optical SLM. The

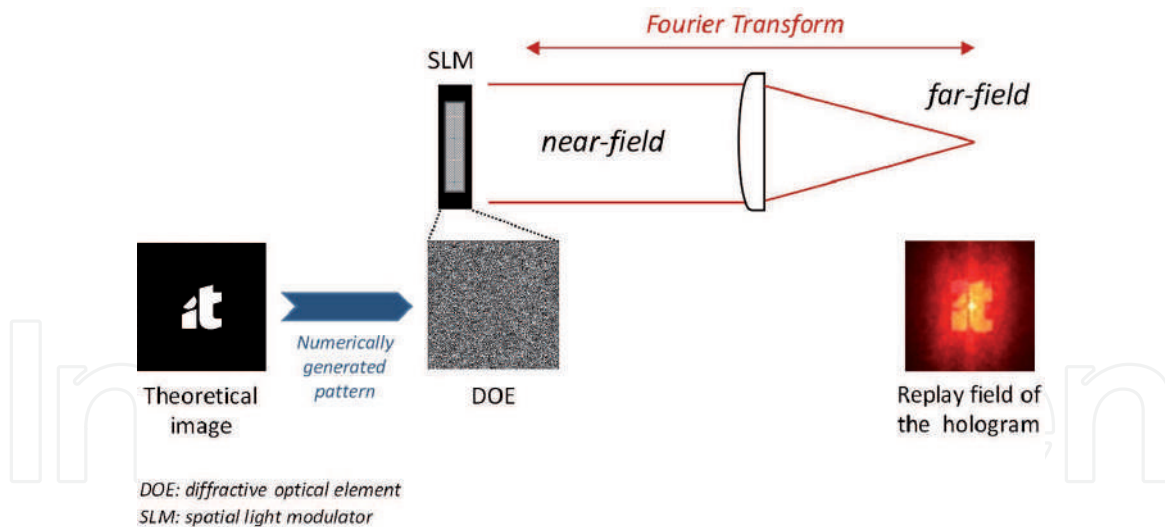


Figure 1.

Diagram of a Fourier transform through a positive lens. A complex design pattern (diffractive optical element (DOE)) is provided to the SLM to generate the expected hologram in the replay field (far field).

modulation material of electro-optical SLM is liquid crystal. Similarly, a liquid crystal SLM has a microdisplay being employed for the incident light modulation and collection. This can be realized in a transmissive form using a liquid crystal display (LCD) SLM technology or in a reflective form with LCoS SLM technology. One of the leading features of the modulators is in the liquid crystal molecule alignment. Typically, this can be either vertical, parallel, or with twisted formation. Consequently, with suitable polarizing optics, this influences the incident light beam properties that can be effectively changed, i.e., amplitude, phase, or their combination [8, 23, 27].

It should be noted that the common hologram generation techniques cannot arbitrarily modulate the beam phase and amplitude concurrently [26, 27]. Therefore, it is unrealistic to basically address the desired pattern inverse Fourier transform into the far field and replicate the resulting amplitude and phase distribution directly on the SLM. As a consequence, the employment of optimization algorithms is highly recommended for evaluating the best potential hologram within the device constraints, e.g., the best pixel distribution in which each pixel will be able to take only one of two states that correspond to a 0 or π phase shift [23, 26].

The nematic LCoS technology is a type of SLM with phase-only modulation capability. Moreover, it is an electrically addressed reflection modulator category in which a direct and accurate voltage controls the liquid crystal and the light beam wave front can be modulated as well [28, 29]. An example of an LCoS SLM is illustrated in **Figure 2** [23]. The LCoS SLM can be employed as a diffractive device for reconstructing images from CGH [30].

CGH can be employed for different communication purposes and has been gaining application in indoor visible light communication systems [31]. Furthermore, suitable holograms can be readily generated by employing a variety of optimization techniques such as iterative Fourier transform algorithm (IFTA) [5, 32–34]; linear Fourier transform (i.e., linear phase mask) [5, 18, 23, 35]; simulated annealing [36]; and Gerchberg-Saxton algorithm [37]. The employment of the SLM as a diffractive device for reconstructing images from CGH permits the light beam wave front to be modulated [8, 23].

As aforementioned, LCoS displays have been gaining significant recognition as promising microdisplays for various types of SLM applications. Similarly, they possess attractive and significant features like very high spatial resolution and

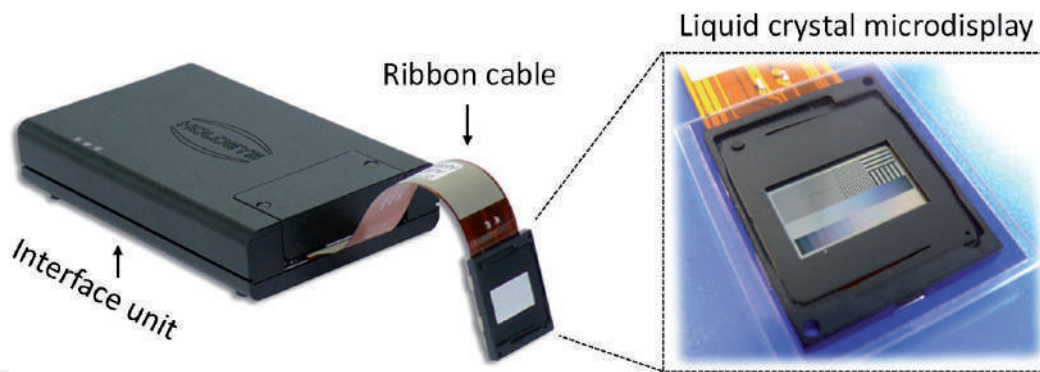


Figure 2.
LCoS SLM Pluto phase modulator from Holoeye© 2018 Holoeye photonics AG.

light efficiency [38]. Due to this, they have been applicable in a plethora of optical contexts such as communication, reconfigurable interconnects [39], storage [40], diffractive optics [41], metrology [42], and quantum computing [43]. They are also applicable in the wave shaper technology for optical signal processing and monitoring [44]. In addition, other advantages of the LCoS are that it is highly cost-effective and can as well be flexibly programmed. This helps in supporting a number of additional functions like group delay ripple compensation, wavelength filtering, and chromatic dispersion compensation. Besides, it can aid in ensuring variable attenuation for individual wavelength channels as well as output ports. Consequently, LCoS device offers a cost-effective and promising solution for the wavelength selective switch (WSS) [40].

The LCoS microdisplay SLM has a good implementation history in the WSS systems. Its employment in the WSS system core component can be attributed to a number of advantages such as larger spatial bandwidth, more port availability, and enhanced resolution, as well as the system miniaturization. The WSS systems have been exploited in the reconfigurable optical add/drop multiplexers (ROADM) in WDM optical networks. It has been observed that ROADM is one of promising schemes that can be employed to improve on the traffic capacity of the existing and future telecommunication systems [40, 45]. Moreover, in communication networks, the ease of adding or dropping the wavelength is essential. They can ensure effective information access or rerouting to another appropriate path in the network. It should be noted that WSS is the ROADM sub-system that has been extensively employed in optical switch applications. In addition, microelectromechanical systems (MEMS) [46] and WSS based on LCoS [47] have been commercialized for different applications. Also, WSS by means of LCoS operates on the principle of “disperse and select,” in which the inward bound WDM channels are dispersed into a distinct wavelength channel and subsequently relayed by LCoS through programmable grating patterns. This is in an attempt to facilitate an add and drop function. It is envisaged that the next-generation ROADM will hold different attractive features such as directionless, colorless, and contentionless in order to improve the system performance [40].

Furthermore, LCoS technology can also be employed in flex grid that has been considered as the major feature for the next-generation networks [40, 48]. It should be noted that the traditional fixed grid with 50 GHz spacing standardized by the International Telecommunication Union (ITU) Telecommunication Standardization Sector (ITU-T) possesses a number of challenges. The fixed grid has been observed to bring about the optical spectra being inefficiently used. Besides, it constrains the system transmission capacity considerably. On the other hand, the flex grid implementation enables the use of different modulation formats

and their coexistence on a shared infrastructure. They can also be densely and efficiently multiplexed which aids the optical networks, not only to extend the reach but also the per channel bit rate. It has also been envisaged that implementation of WSS and SDM will significantly help further in extending the network reach and capacity [40].

3. Methodology

The adopted methodology to implement the SLM flexible platform for optical systems can be subdivided into two main sections: (i) the algorithms employed for the CGH generation and optimization methodology (in Section 3.1) and (ii) the SLM framework setup implementation with application in SDM systems and characterization/testing of PIC (in Section 3.2).

The framework ability to improve the overall alignment process and excite different cores of a MCF, can provide a valuable contribution for the impairment mitigation of the system optical path, which can relax digital signal processing (DSP) equalization requirements of the SDM system [5, 18, 22, 34, 49].

Furthermore, its use as a flexible platform for feeding photonic integrated processors was also explored for the characterization/test of PICs, and results have been presented for its implementation as a parallel implementation of the Haar transform (HT) image compression algorithm [8, 18, 23].

3.1 CGH pattern establishment

Holography is a 3D-based display system that comprises exploiting diffraction and interference for recording and reconstructing optical wave fronts. Moreover, computer-generated holography is an effective technique that is appropriate for a broad variety of displays such as two-dimensional (2D), volumetric, autostereoscopic, stereoscopic, and true 3D imaging. It is remarkable that the CGH is becoming feasible due to the emergence of progressively powerful computers that prevents the conventional interferometric recording step in the formation of hologram [50]. In addition, the CGH can be viewed as a phase mask with spatially variable transmittance or a diffractive optical element that can be readily displayed on the devices such as SLM, which are capable of diffracting light [5, 51]. Also, the information that needs to be transformed is presented to an optical system, through the SLM. This is effected with a suitable phase mask for the concerned input function [25].

From a set of different available techniques for the generation of CGH (e.g., IFTA, linear Fourier transform, simulated annealing, and Gerchberg algorithm, as described in Section 2), in our SLM framework, higher focus was given to the linear Fourier transform principle for the calculus of the numerical interference patterns to generate the holograms (CGH). This decision was mainly due to the intensive computational requests and high power loss (up to 9 dB [26]) associated with the implementation of the simulated annealing and Gerchberg-Saxton algorithms and additional computational cost of IFTA when compared to linear phase mask.

Thus, a simplified approach based on the implementation of a linear phase mask generation (in Section 3.1.1) and the development of a new iterative algorithm experimentally driven for CGH effective optimization (in Section 3.1.2) is proposed and tested.

All algorithms were developed and implemented in MATLAB© [52].

3.1.1 Linear phase mask CGH

A linear phase mask can be described as a numerical information transformation (in the Fourier domain) of the input function of interest [25], which can be introduced into the optical system through an SLM.

The CGH implemented with a linear phase mask can be expressed in the frequency domain as expressed in Eq. (1) [5, 23], where f_x and f_y denote the spatial frequency vector components that correspond to the image to be generated in both X and Y axes, respectively, and c_x and c_y represent the horizontal and vertical tilt parameters, respectively.

$$M_{linear} = M(f_x, f_y) = -2\pi(c_x f_x + c_y f_y) \quad (1)$$

A collimated Gaussian beam with transverse profile S_{in} is imaged onto the SLM via a lens, Eq. (2), where (x_0, y_0) offer the horizontal and vertical position, respectively, and (w_x, w_y) represent the width and the height of the beam, respectively, as depicted in **Figure 3** [8].

$$S_{in} = \exp\left(-\left(2\frac{x-x_0}{w_x \log(\sqrt{2})}\right)^2 - \left(2\frac{y-y_0}{w_y \log(\sqrt{2})}\right)^2\right) \quad (2)$$

With the adoption of Fraunhofer approximation, the Fourier transform is produced on the SLM plane, $fft(S_{in})$. Afterward, the subsequent illumination profile is multiplied with the phase mask, $e^{iH_{mask}}$. The resultant signal is then Fourier transformed via the second lens by means of an inverse Fourier transform to achieve the output signal S_{out} , which can be defined as Eq. (3) [5, 8]:

$$S_{out} = ifft(H(fft(S_{in}))) \quad (3)$$

A graphical user interface (GUI) was also developed to test different masks to be applied to the SLM device [18] (see **Figure 4**).

Different phase masks can be attained by adjusting the different available parameters from the developed GUI. For the *Input Beam* GUI panel the following

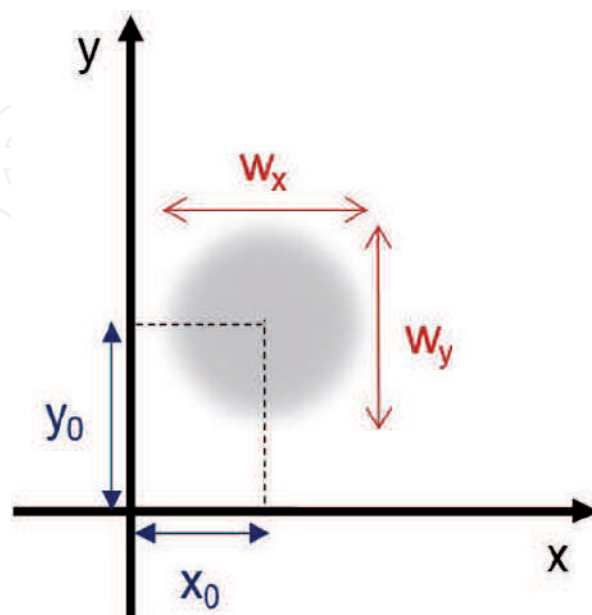


Figure 3. Cartesian coordinate system description of the parameters (x_0, y_0) and (w_x, w_y) employed for the input beam S_{in} estimation [8].

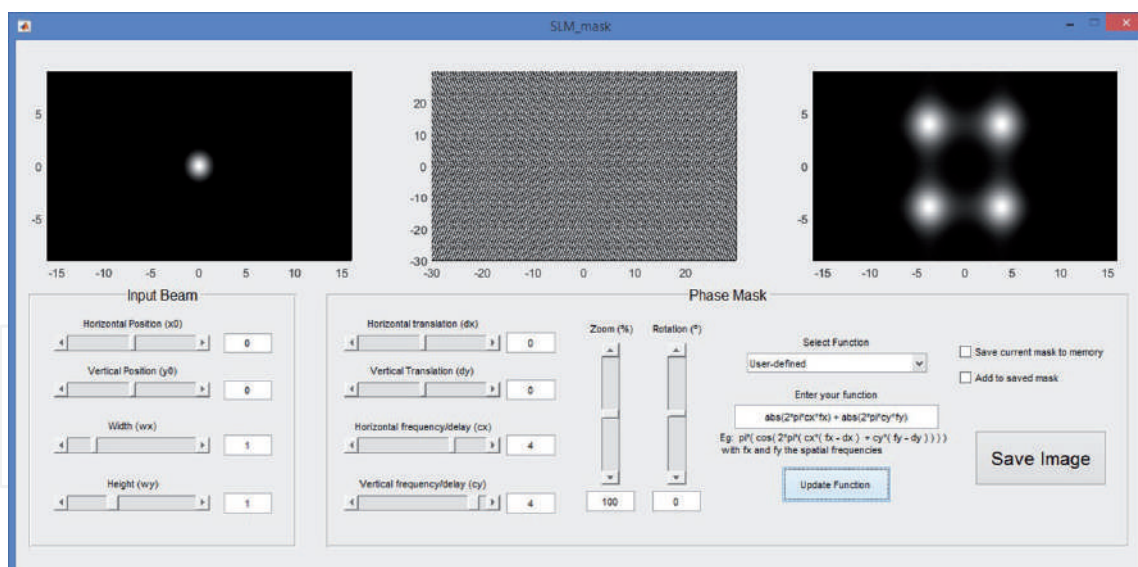


Figure 4. GUI *SLM_mask* to generate the different phase masks applied to the SLM [18].

input parameters are available: (i) horizontal position (x_0); (ii) vertical position (y_0); (iii) width of the beam (w_x); and (iv) height of the beam (w_y) (see GUI panel *Input Beam* in the **Figure 4**).

$$S_{out} = \text{ifft}(H(\text{fft}(S_{in}))) \quad (4)$$

The Phase Mask GUI panel offers the correspondent input parameters: (i) horizontal translation (d_x); (ii) vertical translation (d_y); (iii) horizontal frequency delay (c_x); (iv) vertical frequency delay (c_y); (v) percentage of zoom (%); (vi) rotation in degrees ($^\circ$); and (vii) selection of three possible input functions, i.e., sinusoidal Eq. (4), linear Eq. (1), or defined by the user (user-defined). The option to save or replace the phase mask file is also made available, as depicted in the Phase Mask GUI panel from **Figure 4**.

The implemented scripts and GUI were written in MATLAB© [52].

3.1.2 Optimization of the linear phase mask CGH

In an effort to realize the hologram that can suitably replicate the output signal, we estimated the hologram of the beam through the image phase-only information of the generated hologram. Thus, a first linear phase mask is generated to produce the expected initial field, i.e., the input function of interest.

Since a phase-only SLM does not permit the inverse Fourier of the desired pattern to be addressed into the far field and replicated into the resultant distribution of amplitude and phase on the SLM directly. It is quite demanding to generate a CGH with guarantees for the light to be spatially modulated with the required accuracy and resolution. To address these challenges and obtain the desired hologram with an error factor $\delta \leq 10\%$, we implemented an iterative algorithm to optimize the generation of the linear phase mask. Also, the error factor threshold was set so as to prevent an infinite loop in the adopted optimization algorithm, while guaranteeing that the output result has an accuracy $\geq 90\%$.

The algorithm was implemented to generate a hologram that replicates the output of the four waveguides (WG) of an optical chip for data compression proposes [8, 23, 53]. A hologram of four beams was calculated by a phase-only

superimposition of four independent holograms generated by Eq. (1). Then, the corresponding linear transformations in the Fourier domain provided in Eq. (5) and Eq. (6) were applied [8, 23]:

$$H = \angle(e^{iH_1} + e^{iH_2} + e^{iH_3} + e^{iH_4}) \quad (5)$$

$$H_1 = \exp(i2\pi(c_{x1}f_x + c_{y1}f_y)) \quad (6)$$

The block diagram of the employed algorithm is given in **Figure 5**, and the major steps of the algorithm are enumerated as follows [23]:

- i. Generate a first linear phase mask to produce the expected initial field based on Eq. (5).
- ii. Initially set the four values a_{1-4} to 1, from $H = \angle(a_1 e^{iH_1} + a_2 e^{iH_2} + a_3 e^{iH_3} + a_4 e^{iH_4})$.
- iii. Acquire the replay field from the hologram generated by SLM (*I* SLM) with a camera, and feed this data to the algorithm.
- iv. Calculate the difference between the hologram generated and the initial field expected, defined as error factor: $\delta = |I_{SLM} - I_1| \leq 0.1$.
- v. If the condition $\delta \leq 0.1$ is not satisfied, repeat steps ii–iv by iteratively adjusting the values of a_{1-4} to compensate for the error factor.

The developed algorithm in MATLAB® is capable of controlling both SLM and camera hardware, providing a dynamic experimentally driven algorithm for effective CGH optimization.

The error factor (δ) is defined to quantify the generated hologram deviation from the optical chip anticipated output [8, 23].

3.2 CGH generation setup

The employed SLM is a reflective LCoS phase-only type, and its model is PLUTO-TELCO-012. It can operate within the wavelength range of

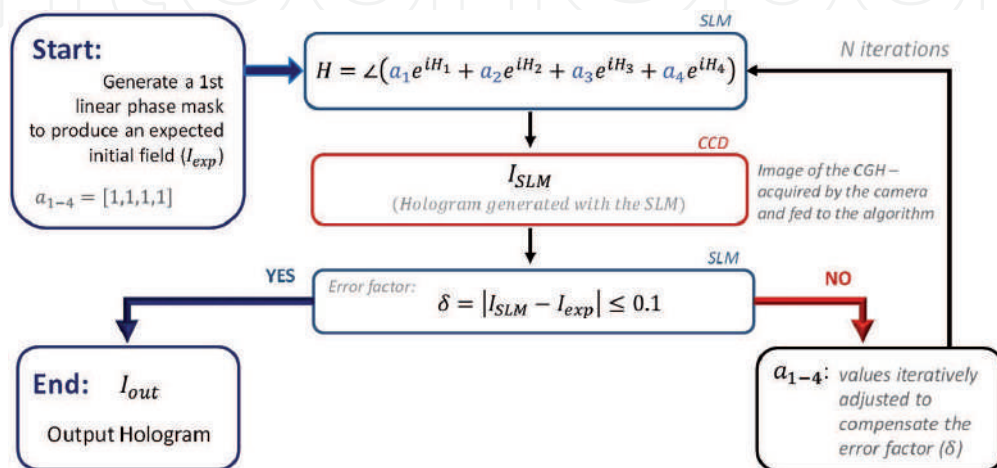


Figure 5. Block diagram of the algorithm applied for the optimization of the linear phase mask CGH [23].

1400–1700 nm. Additionally, an active area of $15.36 \times 8.64 \text{ mm}^2$, a pixel pitch of $8.0 \text{ }\mu\text{m}$, a 92% fill factor, and 80% reflectivity are employed for displaying the generated hologram.

Two different setup arrangements were implemented to create CGH for SDM (e.g., MCF) and PIC applications.

3.2.1 CGH setup for SDM

Setup alignments were carried out, using a red laser of 637 nm (power 70 mW, SM fiber-pigtailed laser diode), a collimator, two lenses, a charge-coupled device (CCD) image sensor, and the LCoS-SLM. After the alignments, an MCF of 10 m of length and a bit error rate (BER) tester were introduced in the setup, as depicted in **Figure 6**.

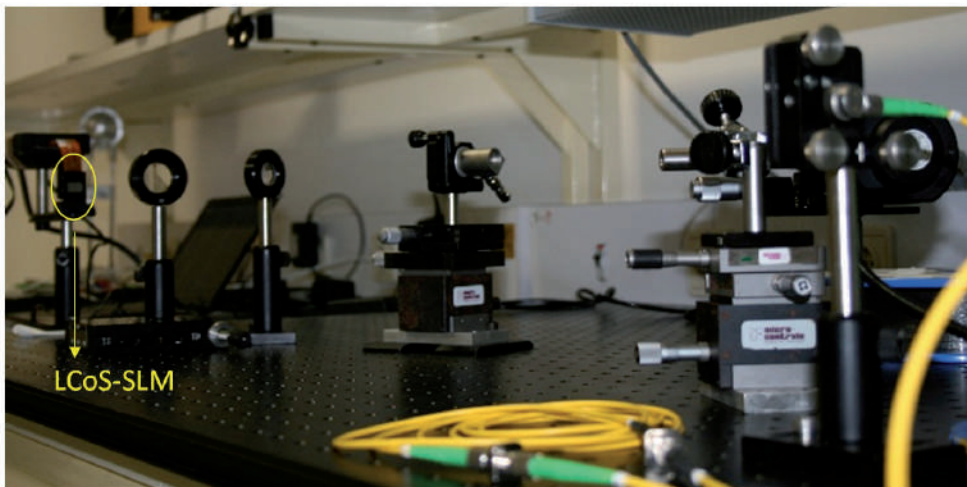
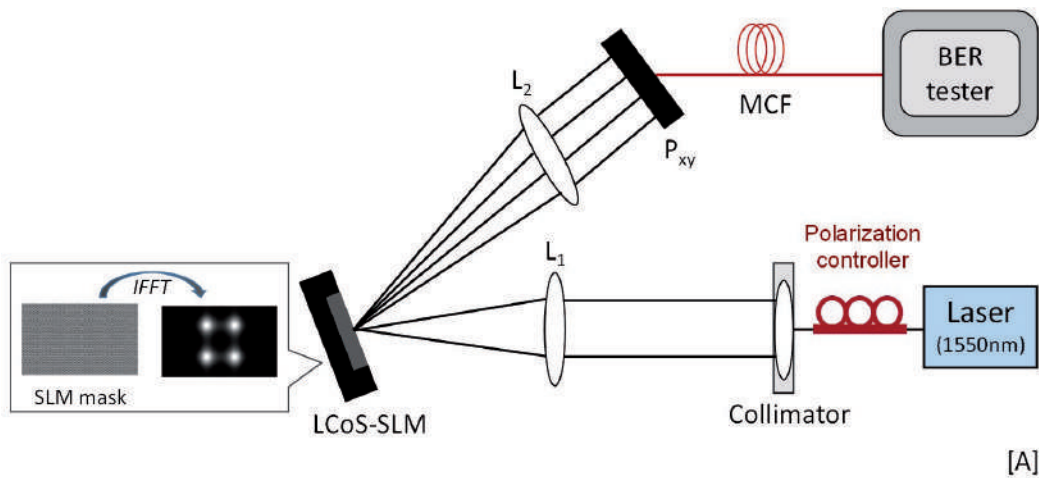


Figure 6. [A] Setup diagram of the SLM platform for MCF applications. [B1, B2] photographs of the setup.

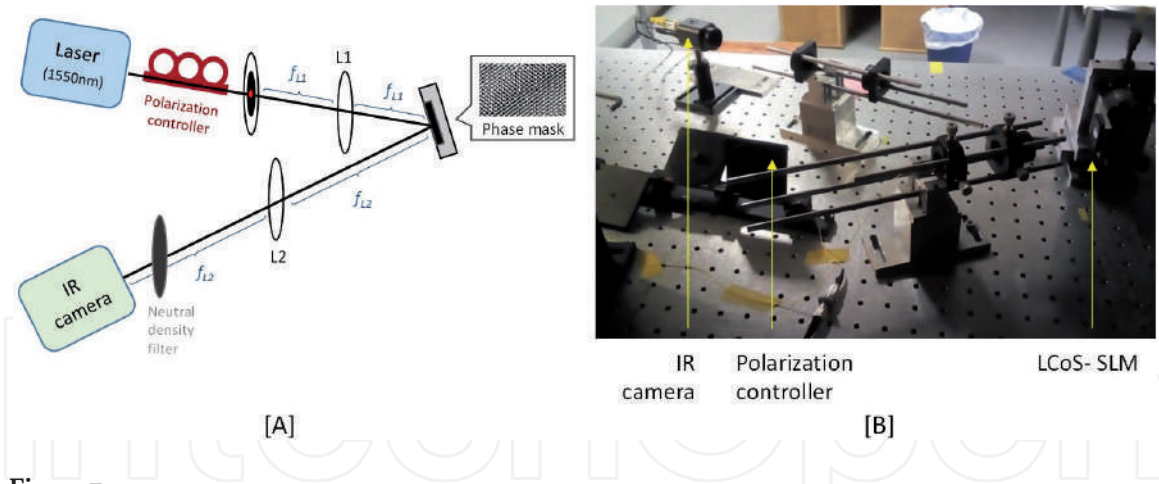


Figure 7.
 [A] Hologram reconstruction scheme using an infrared (IR) laser of 1550 nm, a polarization controller, lens L1, an LCoS-SLM, lens L2, and an IR camera. [B] Photography of the presented setup.

The MCF contained four cores arranged in a quadrangular lattice pattern, with a side length of $36.25 \mu\text{m}$ and attenuation @1550 nm of 0.45 dB/km.

The nonreturn-to-zero (NRZ) signal was generated by a pattern generator (Agilent N4901B) using a pseudorandom binary sequence (PRBS) $2^{31}-1$. This signal was injected to the tunable direct modulator laser to create 10 Gb/s optical signal. After the MCF, the signal was detected by avalanche photodiode (APD) receiver inside the small form-factor pluggable (SFP) transceiver.

3.2.2 CGH setup for PIC

In an effort to eliminate the phase distortion and enable the full Fourier transform scale by the focal length (f) factor, the optical system is designed based on the $4f$ system configuration. The implementation is the basis of a low distortion optical system.

The setup consists of devices such as two lenses (AC254-050-C-ML, AR coating 1050-1620 nm) L1 and L2 with a focal length of 75 and 250 mm, respectively; polarization controller; an infrared (IR) laser of 1550 nm (wavelength); a near-infrared (1460-1600 nm) camera (sensing area, $6.4 \times 4.8 \text{ mm}$; resolution, 752×582 ; pixel size, $8.6 \times 8.3 \mu\text{m}$) for capturing the produced hologram; and a neutral density filter, to prevent saturation in the camera acquisition (see **Figure 7**) [8, 23].

4. Results and discussion

In this section, we present the experimental CGH results obtained for the SDM and PIC applications.

4.1 SLM platform for MCF

A BER of 1.2×10^{-3} was measured in the experiment described in Section 3.2.1. Test result shows an error-free transmission below the BER limit of 3.8×10^{-3} (7% hard-decision FEC) [54, 55] threshold.

Thus, the SLM framework was able to properly function as a spatial coupling interface between the SLM generated pattern and the MCF cores. The platform allows an easy adjustment of the generated phase mask (CGH), contributing to an effective dynamic optimization of the MCF fiber transmission [18].

Future work will be performed in order to optimize the current convergence, namely, improve the optical system components (e.g., lenses and collimator) and the implemented phase masks [18].

4.2 CGH for PIC applications

An integrated approach for compression applications implemented in an indium phosphide (InP) optical chip was fabricated to realize a Haar wavelet transform [53]. The HT is a wavelet-based method with promising attributes for compression transformation techniques. Their application in image processing and pattern recognition due to its simple design, fast computation power, and efficiency can be easily realized by optical planar interferometry [53, 56, 57].

The HT operations include low-pass (L) and high-pass (H) filters applied over one dimension at a time. This filtering operation corresponds to the calculation of the average between two neighbors' pixel values (LP) or the difference between them (HP) [57]. The HT is implemented with a two-level network composed by three asymmetric adiabatic couplers (AAC) 2×2 , reproducing the required operations, i.e., the average (sum) and the difference (subtraction) between the optical input pair [53]. The 2D HT can be decomposed in four sub-bands, LL, LH, HL, and HH [57]. The LL gives the data compressed.

In the optical chip (or PIC), these four sub-bands can be extrapolated from the four output WG at the end of the three AAC network, as depicted in **Figure 8**.

The optical chip is composed of four distributed feedback (DFB) source lasers (L_1 – L_4), three asymmetric adiabatic coupler (AAC₁–AAC₃), six positive-intrinsic-negative (PIN) photodiodes for network monitoring, six MMI splitters 1×2 , one MMI splitter 2×2 , and two spot size converters (SSC), at the correspondent HT network output LL (compression) and HH. Further details about the PIC can be found elsewhere [23, 53].

In the described SLM framework, the hologram is generated in an attempt to create the beam profile in the first order of diffraction when being displayed on the SLM. The CGH is expected to reproduce the four WG outputs of the PIC implementing the HT [23, 53] (see **Figure 8**).

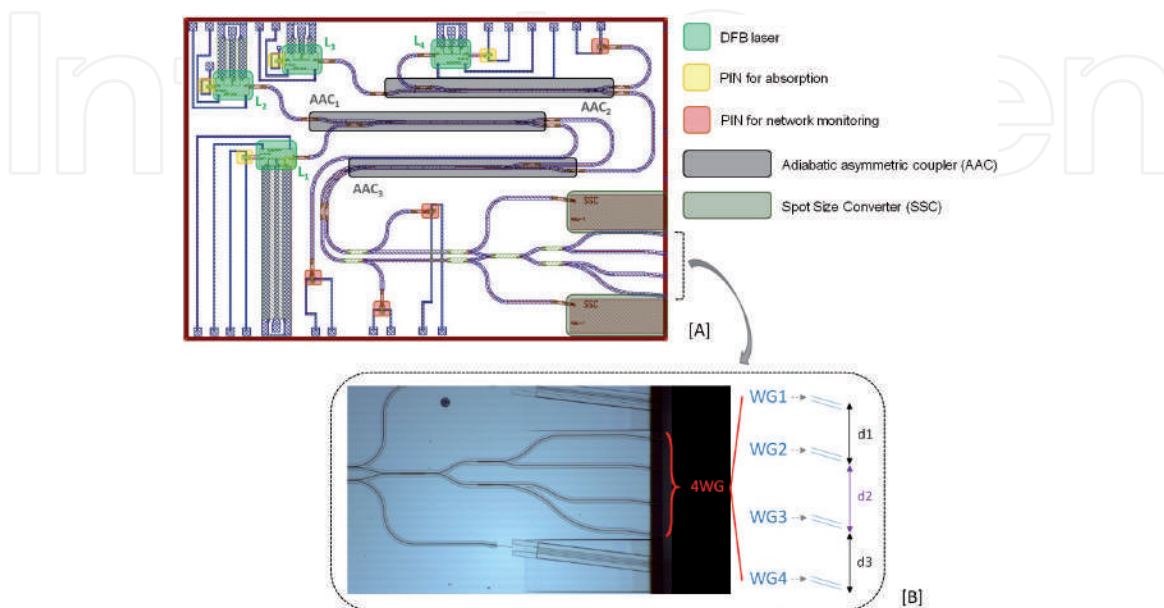


Figure 8.

[A] Design architecture of the PIC for data compression based on HT. [B] Measurements of the distance between the four WG at the end of the two-level compression network of the PIC [23].

In **Figure 9**, we present the obtained image from the hologram replay field generated with the initial (I_1) and optimized (I_{out}) CGH [8, 23].

The analysis of the obtained replay field images can be described by the steps described below:

- i. Calculate the intensity integration of the image matrix, i.e., the sum of all elements along each line of the image matrix, depicted as S_{row} .
- ii. Application of the Savitzky–Golay (SG) filter to smoothen the intensity integration signal obtained in step (1), depicted as S_{SG} .
- iii. Implementation of a first-order Gaussian fit curve to the filtered signal, depicted as *Gauss fit*.
- iv. Extraction of Gaussian parameters to calculate the distances between the four beams (obtained from the CGH) and compare with the expected results (d_1 , d_2 , and d_3 from the optical chip).

Results from the integrated intensity profile of the replay field after the CGH optimization, i.e., after step (3), are presented in **Figure 10**.

The distance between the four beams was calculated from the center position of each beam profile, given by the Gaussian fit coefficient corresponding to the position of the center of the peak. The coefficients were obtained with 95% confidence bounds [23]. The deviation values (δ) between the generated holograms (i.e., initial I_1 and optimized I_{out}), when compared with the expected output of the optical chip (i.e., d_1 , d_2 and d_3 from **Figure 8**), are presented in **Table 1** [23].

The measured power of the beams obtained by the integration intensity profiles is depicted in **Table 2** [23].

An improved hologram is achieved with the optimization of the linear phase mask CGH, i.e., with a reduction of up to 11% in the error factor (between

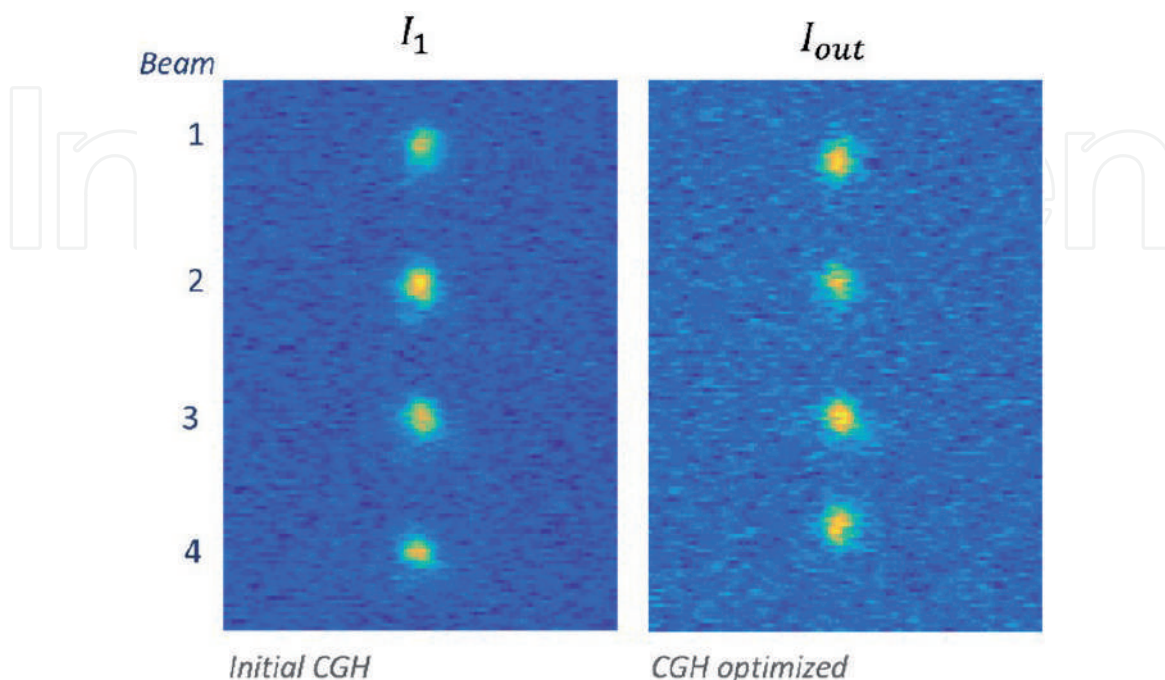


Figure 9. Hologram replay field obtained by the IR camera with an (i) initial hologram (left figure) and (ii) optimized hologram (right figure).

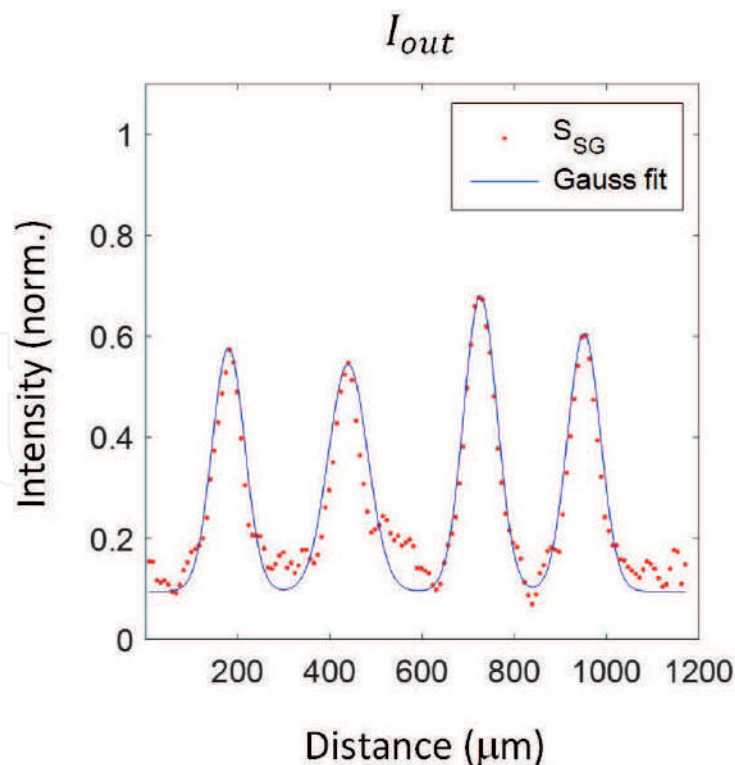


Figure 10. Gaussian fit (Gauss fit, blue line) of smoothed integrated intensity signal from the replay field image (S_{SG} , red dots) of final optimized CGH [23].

	Initial CGH (%)	Optimized CGH (%)
δ_{d1}	19.76	7.48
δ_{d2}	1.96	2.90
δ_{d3}	14.31	9.44

Table 1. Error factor (δ) values for d_1 , d_2 , and d_3 .

Beam	Initial CGH (u.a.)	Optimized CGH (u.a.)
1	6.30	5.12
2	8.21	5.78
3	7.18	6.37
4	7.69	5.51
Mean	7.35 ± 0.81	5.69 ± 0.52
Std (%)	11.17	9.14

Table 2. Integration of the intensity profiles for the four beams.

initial and optimized holograms). Nonetheless, the loss of 1.1 dB identified on the mean beam power for the optimized CGH, an improved equalization between the beams was observed, with a 2% reduction in the standard deviation [23].

Algorithm improvements should be implemented to mitigate the power discrepancies between the four beams and optical artifacts associated with the diffraction of light, with the objective of mitigating the signal loss at the output of the optical chip.

A possible approach to correct some of these artifacts can be the application of the Gerchberg-Saxton [37] or simulated annealing [36] algorithms; nonetheless, due to the power loss (up to 9 dB [26]) associated with these approaches, they were not addressed in this implementation [23].

The phase mask that replicates the expected output of the PIC optical operation can be used to multiplex/demultiplex the obtained result. Furthermore, a phase mask, which addresses the HT operations, can also be applied to invert the compression induced by the HT (optically implemented in the PIC all-optical network with three AAC). Thus, a proof of concept of the PIC operation through the SLM coupling framework is expected [8, 23].

5. Conclusion

LCoS SLM technology implementation has been gaining importance in optical system applications, like telecom with the development of high-capacity optical components in system functionalities as switching (in ROADMs), multiplexing and demultiplexing, and optical signal processing. In this chapter, a proof of concept on the implementation of a new SLM-based flexible coupling platform has been provided. We have also explored its implementation for applications in SDM systems and PIC characterization/testing. Furthermore, optimized methodologies to generate the CGH were developed and implemented. Main results include (i) $BER = 1.2 \times 10^{-3}$ for a SDM system, i.e., the use of the SLM to efficiently excite the different cores of a MCF, and (ii) CGH ($\delta \leq 1.5\%$) to feed/receive the output of an optical chip for data compression based on the HT. The demonstrations pave the way for the potential use of the SLM flexible platform in the development of multidimensional optical systems, by providing a versatile optical method which can overcome impairments introduced by the optical path in a MCF (e.g., by improving the setup alignment and excitation of different cores in MCF) and deliver a more robust optical methodology to assess and test photonic processors (e.g., offering a proof of concept of the PIC HT operation).

Acknowledgements

This work is funded by Fundação para a Ciência e a Tecnologia (FCT) through national funds under the scholarship PD/BD/105858/2014. It is also supported by FCT/MEC/MCTES and when applicable co-funded by FEDER – PT2020 partnership agreement under the project COMPRESS – PTDC/EEI-TEL/7163/2014 and the project UID/EEA/50008/2019. The authors acknowledge PICadvanced for its collaboration.

IntechOpen

Author details

Cátia Pinho^{1,2*}, Isiaka Alimi^{1,2}, Mário Lima^{1,2}, Paulo Monteiro^{1,2}
and António Teixeira^{1,2}

1 Instituto de Telecomunicações (IT), University of Aveiro, Aveiro, Portugal

2 Department of Electronics, Telecommunications and Informatics (DETI),
University of Aveiro, Aveiro, Portugal

*Address all correspondence to: catiap@ua.pt

IntechOpen

© 2019 The Author(s). Licensee IntechOpen. This chapter is distributed under the terms of the Creative Commons Attribution License (<http://creativecommons.org/licenses/by/3.0>), which permits unrestricted use, distribution, and reproduction in any medium, provided the original work is properly cited. 

References

- [1] He J et al. A survey on recent advances in optical communications. *Computers and Electrical Engineering*. 2014;**40**(1):216-240
- [2] Ericsson. Ericsson Mobility Report. 2018
- [3] Winzer PJ. Spatial multiplexing in fiber optics: The scaling of metro/core capacities. *Bell Labs Technical Journal*. 2014;**19**:22-30
- [4] Ayyash M et al. Coexistence of WiFi and LiFi toward 5G: Concepts, opportunities, and challenges. *IEEE Communications Magazine*. 2016;**54**(2):64-71
- [5] Pinho C, Shahpari A, Alimi I, Lima M, Teixeira A. Optical transforms and CGH for SDM systems. In: 18th International Conference on Transparent Optical Networks (ICTON 2016). 2016. pp. 1-4
- [6] Alimi IA, Monteiro PP, Teixeira AL. Outage probability of multiuser mixed RF/FSO relay schemes for heterogeneous cloud radio access networks (H-CRANs). *Wireless Personal Communications*. 2017;**95**(1):27-41
- [7] Alimi IA, Monteiro PP, Teixeira AL. Analysis of multiuser mixed RF/FSO relay networks for performance improvements in cloud computing-based radio access networks (CC-RANs). *Optics Communication*. 2017;**402**:653-661
- [8] Pinho C et al. Flexible platform for feeding photonic integrated processors. In: The Thirteenth Advanced International Conference on Telecommunications (AICT 2017). 2017. pp. 1-4
- [9] Grand View Research. Photonic Integrated Circuit (IC) Market Size Report. 2016
- [10] Credence Research. Photonic Integrated Circuits Market. 2016
- [11] Desurvire E et al. Science and technology challenges in XXIst century optical communications. *Comptes Rendus Physique*. 2011;**12**(4):387-416
- [12] Ip E, Kahn JM. Increasing optical fiber transmission capacity beyond next-generation systems. In: LEOS 2008. 21st Annual Meeting of the IEEE Lasers and Electro-Optics Society 2008. pp. 606-607
- [13] Shannon CE. A mathematical theory of communication. *Bell System Technical Journal*. 1948;**27**(3):379-423
- [14] Alimi I, Shahpari A, Sousa A, Ferreira R, Monteiro P, Teixeira A. Challenges and opportunities of optical wireless communication technologies. In: *Optical Communication Technology*. London: IntechOpen; 2017. p. 41
- [15] Richardson DJ, Fini JM, Nelson LE. Space-division multiplexing in optical fibres. *Nature Photonics*. 2013;**7**(5):354-362
- [16] Yuan H, Furdek M, Muhammad A, Saljoghei A, Wosinska L, Zervas G. Space-division multiplexing in data center networks: On multi-Core fiber solutions and crosstalk-suppressed resource allocation. *Journal of Optical Communications and Networking*. 2018;**10**(4):272
- [17] Morita I, Igarashi K, Tsuritani T. 1 Exabit/s·km transmission with multi-core fiber and spectral efficient modulation format. In: 2014 OptoElectronics and Communication Conference and Australian Conference on Optical Fibre Technology. 2014. pp. 316-318
- [18] Pinho C et al. Spatial light modulator based flexible coupling platform for applications in SDM and PIC. In: 20th European Conference on Integrated Optics (ECIO 2018). 2018. pp. 238-240

- [19] Richardson DJ. Unleashing the spatial domain in optical fiber communications. In: 2013 IEEE Photonics Society Summer Topical Meeting Series. 2013. pp. 70-71
- [20] Essiambre R-J, Tkach RW. Capacity trends and limits of optical communication networks. *Proceedings of the IEEE*. 2012;**100**(5):1035-1055
- [21] Carpenter J, Leon-Saval S, Eggleton BJ, Schröder J. Spatial light modulators for sub-systems and characterization in SDM. In: 2014 OptoElectronics and Communication Conference and Australian Conference on Optical Fibre Technology. 2014. pp. 23-24
- [22] Lee HJ, Moon HS, Choi S-K, Park HS. Multi-core fiber interferometer using spatial light modulators for measurement of the inter-core group index differences. *Optics Express*. 2015;**23**(10):12555
- [23] Pinho C et al. Flexible spatial light modulator based coupling platform for photonic integrated processors. *International Journal on Advances in Telecommunications*. 2018;**11**(1):20-31
- [24] Smit M et al. An introduction to InP-based generic integration technology. *Semiconductor Science and Technology— IOPscience*. 2014;**29**(83001):1-41
- [25] Goodman JW. *Introduction to Fourier Optics*. 2nd ed. Stanford: McGraw-Hill Companies; 1996
- [26] Carpenter J. *Holographic Mode Division Multiplexing in Optical Fibres*. Cambridge, UK: University of Cambridge; 2012
- [27] Lazarev G, Hermerschmidt A, Kr S. LCOS spatial light modulators: Trends and applications. In: *Optical Imaging and Metrology: Advanced Technologies*. Weinheim: Wiley-VCH. 2012. pp. 1-29
- [28] Holoeye. “Spatial Light Modulators,” Holoeye Photonics AG. 2013. [Online]. Available: <http://holoeye.com/spatial-light-modulators/> [Accessed: 22-11-2017]
- [29] Hamamatsu. Phase spatial light modulator LCOS-SLM. In: *Opto-Semiconductor Handbook*. Tokyo: Hamamatsu Photonics. 2012. pp. 1-14
- [30] Kovachev M et al. Reconstruction of computer generated holograms by spatial light modulators. In: *Multimedia Content Representation, Classification and Security*. Vol. 4105. Berlin Heidelberg: Springer; 2006. pp. 706-713
- [31] Younus SH, Hussein AT, Alresheedi MT, Elmirghani JMH. CGH for indoor visible light communication system. *IEEE Access*. 2017;**5**:24988-25004
- [32] Torii Y, Balladares-Ocana L, Martinez-Castro J. An iterative Fourier transform algorithm for digital hologram generation using phase-only information and its implementation in a fixed-point digital signal processor. *Optik (Stuttgart)*. 2013;**124**(22):5416-5421
- [33] Ripoll O, Kettunen V, Herzig HP. Review of iterative Fourier-transform algorithms for beam shaping applications. *Optical Engineering*. 2004;**43**(11):2549-2556
- [34] Pinho C, Lima M, Teixeira A. Optical compensation approach for SDM systems. In: *XIII Symposium on Enabling Optical Networks and Sensors (SEONs 2016)*. 2016
- [35] Lesem LB, Hirsch PM, Jordan JA. The Kinoform: A new wavefront reconstruction device. *IBM Journal of Research and Development*. 1969;**13**(2):150-155
- [36] Carpenter J, Wilkinson TD. Graphics processing unit-accelerated holography by simulated annealing. *Optical Engineering*. 2010;**49**(9):095801-095807

- [37] Gerchberg R, Saxton WO, Gerchberg BRW, Saxton WO. A practical algorithm for the determination of phase from image and diffraction plane pictures. *Optik (Stuttgart)*. 1972;**35**(2):237-246
- [38] Collings N, Davey T, Christmas J, Chu D, Crossland B. The applications and technology of phase-only liquid crystal on silicon devices. *Journal of Display Technology*. 2011;**7**(3):112-119
- [39] Roelens MAF et al. Dispersion trimming in a reconfigurable wavelength selective switch. *Journal of Lightwave Technology*. 2008;**26**(1):73-78
- [40] Wang M et al. LCoS SLM study and its application in wavelength selective switch. *Photonics*. 2017;**4**(2):22
- [41] Turunen J, Wyrowski F. *Diffraction Optics for Industrial and Commercial Applications*. Berlin: John Wiley & Sons; 1997
- [42] Osten W, Kohler C, Liesener J. Evaluation and application of spatial light modulators for optical metrology. In: *Óptica Pura y Aplicada, Reunión Española de Optoelectrónica, OPTOEL'05*. 2005. pp. 71-81
- [43] Varga JJM et al. Preparing arbitrary pure states of spatial qubits with a single phase-only spatial light modulator. *Journal of Physics Conference Series*. Apr. 2015;**605**(1):012035-012036
- [44] Schroder J, Roelens MAF, Du LB, Lowery AJ, Eggleton BJ. LCOS based waveshaper technology for optical signal processing and performance monitoring. In: *17th Opto-Electronics and Communications Conference, 2012*. 2012. pp. 859-860
- [45] Keyworth BP. ROADM subsystems and technologies. In: *OFC/NFOEC Technical Digest. Optical Fiber Communication Conference, 2005*. Vol. 3. 2005. p. 4
- [46] de Hennin S, Wall P, Moffat SH, Keyworth BP, Colbourne PD. Addressing manufacturability and reliability of MEMS-based WSS. In: *OFC/NFOEC 2007—Conference on Optical Fiber Communication and the National Fiber Optic Engineers Conference; 2007*; pp. OWV1-3
- [47] Strasser TA, Wagener JL. Wavelength-selective switches for ROADM applications. *IEEE Journal of Selected Topics in Quantum Electronics*. 2010;**16**(5):1150-1157
- [48] Shiraiwa M, Furukawa H, Miyazawa T, Awaji Y, Wada N. High-speed wavelength resource reconfiguration system concurrently establishing/removing multiwavelength signals. *IEEE Photonics Journal*. 2016;**8**(2):1-7
- [49] Lhermite J, Suran E, Kermene V, Louradour F, Desfarges-Berthelemot A, Barthélémy A. Coherent combining of 49 laser beams from a multiple core optical fiber by a spatial light modulator. *Optics Express*. 2010;**18**(5):4783-4789
- [50] Slinger C, Cameron C, Stanley M. Computer-generated holography as a generic display technology. *IEEE Computer Society*. 2005;**38**(8):46-53
- [51] Tricoles G. Computer generated holograms: An historical review. *Applied Optics*. 1987;**26**(20):4351
- [52] MathWorks. R2018b—MATLAB and Simulink Product Families. The MathWorks, Inc. [Online]. Available: https://www.mathworks.com/products/new_products/latest_features.html [Accessed: 13-04-2019]
- [53] Pinho C, Neto B, Morgado TM, Neto H, Lima M, Teixeira A. InP AAC for Data Compression Applications. *IET Optoelectronics*. 2019;**13**(2):67-71

[54] Chang F, Onohara K, Mizuochi T. Forward error correction for 100 G transport networks. *IEEE Communications Magazine*. 2010;**48**(3):S48-S55

[55] Matiss A et al. Performance of an integrated coherent receiver module for up to 160G DP-QPSK transmission systems. *Journal of Lightwave Technology*. 2011;**29**(7):1026-1032

[56] Ashok V, Balakumaran T, Gowrishankar C, Vennila ILA, Kumar AN. The fast Haar wavelet transform for signal & image processing. *International Journal of Computer Science and Information Security*. 2010;**7**(1):126-130

[57] Parca G, Teixeira P, Teixeira A. All-optical image processing and compression based on Haar wavelet transform. *Applied Optics*. 2013;**52**(12):2932-2939

IntechOpen